

Properties of Nanogenerator Materials for Energy-Harvesting Application

W.H. Abd. Majid^{1,*}, N. Ahmad^{1,2}, A.K. Rosli¹, M.A. Mohd Sarjidan¹ and N.A. Halim²

¹Low Dimensional Materials Research Centre, Department of Physics, Faculty of Science, Universiti Malaya, 50603 Kuala Lumpur, Malaysia

²Physics Department, Centre for Defence Foundation Studies, Universiti Pertahanan Nasional Malaysia, 57000 Sungai Besi, Kuala Lumpur, Malaysia

Abstract: Advancements in nanotechnology and materials science have led to the development of a variety of nanogenerator materials with improved properties, making energy harvesting technologies increasingly viable for various applications, such as powering wearable devices, remote sensors, and even small electronic gadgets in the future. The evolution of hybrid materials consisting of polymers and nanoparticles as efficient energy harvesters and energy storage devices is in high demand nowadays. Most investigations on organic ferroelectric P(VDF-TrFE) as a polymer host of polymer nanocomposite devices were primarily focused on the β phase due to its excellent electrical properties for various application purposes. Nanofiller is also introduced into the polymer host to produce a polymer nanocomposite with enhanced properties. A brief description of various physical quantities related to ferroelectric, dielectric, pyroelectric effects and Thermally Stimulated Current (TSC) for energy harvesting applications in nanogenerator materials is presented. This article explores the different materials and uses of various nanogenerators. It explains the basics of the pyroelectric effect and the structure of pyroelectric nanogenerators (PNGs), as well as recent advancements in micro/nanoscale devices. Additionally, it discusses how the performance of ferroelectric, dielectric, pyroelectric, and TSC are impacted by the annealing treatment of P(VDF-TrFE) polymer.

Keywords: Polarization, P(VDF-TrFE), Ferroelectric, Pyroelectric, Thermally Stimulated Current (TSC).

1. INTRODUCTION

The advancement of smart materials with excellent properties, lower cost and low dimensions is essential in designing energy-harvesting nanogenerators. Research in energy conversion has grown rapidly to harness the waste of energy sources in the environment. Energy harvesting conversion mechanisms are exploited such as piezoelectric, pyroelectric, triboelectric and others. The potential of nanogenerators to power small electronic devices and sensors is being driven by advances in nanotechnology and materials science. The effectiveness and viability of these devices for harvesting applications are greatly influenced by the characteristics or properties of the materials used in nanogenerators. Pyroelectric nanogenerators (PNGs) are a type of energy-harvesting device that harvests energy using the pyroelectric effect. A material's ability to generate a temporal voltage with time corresponds to the temperature fluctuation that is based on polarization, called the pyroelectric effect. The pyroelectric effect is usually observed in polymeric materials. PNGs offer several advantages, including the ability to harvest energy from naturally occurring temperature fluctuations and integrate into many applications such as self-powered sensors, wearable devices [1] and Internet of Things (IoT) devices [2,3]. At present, researchers are extensively studying a hybrid energy harvesting system that utilizes a triboelectric

nanogenerator (TENG) [4-8]. TENG is a technology that merges the principles of triboelectricity with other energy harvesting methods to capture mechanical energy from various sources and convert it into electrical energy. For instance, a solar panel and piezoelectric generator can be incorporated to harvest energy from sunlight and mechanical vibrations, respectively. This integration enables the system to draw energy from multiple sources, enhancing its efficiency and reliability. However, creating efficient TENGs can be a complicated process, and developing TENGs is more challenging than some other energy harvesting technologies. To achieve optimal triboelectric pairings, careful engineering and experimentation are necessary to identify the right materials and geometries for specific applications [9]. In recent years, several designs of triboelectric, piezoelectric, electromagnetic, and pyroelectric energy harvesters have been introduced, based on biocompatible and eco-friendly natural materials [10-13].

The evolution of hybrid materials consisting of polymers (organic) and nanoparticles (inorganic) as efficient energy harvesters and energy storage devices is of critical importance these days. The polymer nanocomposites are categorized as hybrid materials which contain nanofillers embedded into the polymer matrix. Spin-coating is a common approach in the deposition of nanocomposite thin films before energy harvesting and energy storage applications. To fabricate a thermal or infrared sensor, a material must have excellent ferroelectric properties, high pyroelectric constant, low dielectric loss, and low specific heat and thermal conductivity [14,15].

*Address correspondence to this author at the Low Dimensional Materials Research Centre, Department of Physics, Universiti Malaya, 50603 Kuala Lumpur, Malaysia; E-mail: q3haliza@um.edu.my

A team of researchers, led by Ojha *et al.*, has developed a flexible device called a piezoelectric nanogenerator (PENG) using ZnO microrods blended with polyvinylidene fluoride (PVDF) through the supersonic spraying method [16]. The PENG was placed on various parts of the human body, such as the elbows, palms, knees, and feet, as shown in Figure 1. To measure the electric signals and performance of the device, a periodic tapping test was conducted under a tapping force of 20 N at 5 Hz. The ZP5-based PENG was found to work effectively as a touch sensor and LED lighting, with a maximum power of $112.5 \mu\text{W}$ obtained at $0.08 \text{ M}\Omega$. The power density of the PENG was $12.5 \mu\text{W cm}^{-2}$ with an area of $3 \text{ cm} \times 3 \text{ cm}$. The study suggests that ZnO micro rods can serve as a nucleating agent that induces strong local interactions on the contact surface with PVDF, promoting β phase transformation in PVDF. Therefore, the PVDF/ZnO composite has the potential to power small electronic devices [16,17].

Current research focuses on the inclusion of nanocrystals or quantum dots (QDs) into polymer matrix for various applications; perovskite quantum dots-embedded polydimethylsiloxane (PQDP) film-based triboelectric nanogenerator (TENG) on the

bottom monocrystalline Si solar cell towards harvesting raindrop energy and solar energy [18], the composite P(VDF-TrFE) doped with CsPbBr_3 QDs for piezoelectric nanogenerators [19] and carbon dots (C-dots) in conducting polymers (polypyrrole (PPy) and polyaniline (PANI)) for energy storage applications [20]. Three main issues must be addressed for any polymer nanocomposite to be useful as an energy harvester as reported in our previous work [21]: the agglomeration of quantum dots (QDs), toxicity and energy harvesting performance. Surface modification using a capping agent is essential for controlling the as-synthesized QD size and preventing rapid agglomeration due to the high surface energy. Therefore, due to the excellent progression in the development of nanogenerators based on QDs, this paper presents the origin and history of ferroelectric materials such as polymer, nanocrystal-semiconductor filler and polymer-quantum dots composites focusing on pyroelectric nanogenerators. The theoretical mechanism that plays a role in the polarization of ferroelectric, dielectric and pyroelectric are discussed in this paper which are important characteristics of energy harvesting nanogenerators. Basic principles and theoretical background of Thermally Stimulated Current will also

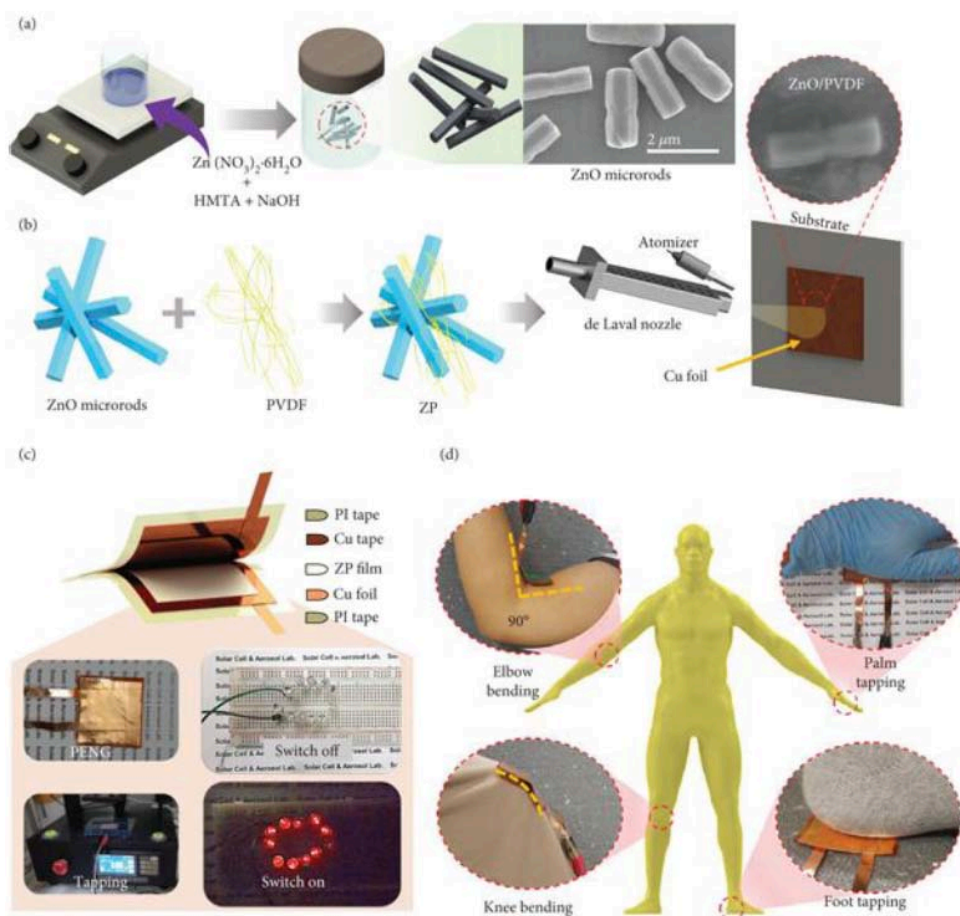


Figure 1: Fabrication process and application of the ZnO/PVDF (ZP)-based PENG (a) synthesis process of ZnO microrods (b) supersonic spraying of the ZP composite (c) fabrication and LED test of ZP5-based PENG (d) energy harvesting using the PENG via body movements [16].

be elucidated as well. This article reviews ongoing research on PVDF-based composites or its copolymer P(VDF-TrFE)-based to improve the efficiency and versatility of pyroelectric nanogenerators for a wider range of applications.

2. FERROELECTRIC CRYSTALS

The ferroelectric and pyroelectric originated from the asymmetry of the crystal structure. The structural symmetry of a crystal depends on its lattice structure and it affects geometrically the structure and physical properties of the crystal such as dielectric, mechanical, piezoelectric, ferroelectric, nonlinear optical properties, etc. [22]. The lattice structure is described by the Bravais unit cell of the crystal. There are only thirty-two macroscopic symmetry types of crystals (32-point groups) and thousands of crystals in nature. The

natural world contains thousands of crystal, with 32 macroscopic symmetry types of crystal as illustrated in Table 1. In a point group, the eight symmetry elements (excluding translation symmetry) consist of rotation axes such as 1 (without rotation), 2 (rotation diad), 3 (rotation triad), 4 (rotation tetrad), 6 (rotation hexad), $\bar{4}$ (rotation-inversion tetrad axis), I (inversion centre) and m (reflection mirror), respectively [22].

Among the 32-point groups, 11-point groups are centrosymmetry with a symmetry centre. A symmetric crystal does not have any polarity and possesses one or more crystallographically unique direction axis. Among these, 20-point groups exhibit piezoelectricity, while 10-point groups have only one unique direction axis. A crystal with point-group symmetry has a unique rotation axis but does not have any mirror perpendicular to this axis. Along a unique rotation axis,

Table 1: Symbol of the 32-point groups on crystallography. Remarks: (*) implies that the piezoelectric effect may be exhibited and (+) implies that pyroelectric and ferroelectric effects may be exhibited (adapted from [22])

Crystal system	International notation	Scönflies' notation	Remarks
Triclinic	1	C_1	*+
	$\bar{1}$	$C_1(S_2)$	-
Monoclinic	2	C_2	*+
	$m(2)$	$C_s(C_{1h})$	*+
	$2/m$	C_{2h}	-
Orthorhombic	2mm	C_{2v}	*+
	222	$D_2(V)$	*
	mmm	$D_{2h}(V_h)$	-
Tetragonal	4	C_4	*+
	$\bar{4}$	S_4	*
	$\bar{4}2m$	$D_{2d}(V_d)$	*
	422	D_4	*
	4mm	C_{4v}	*+
	$4/m$	C_{4h}	-
	$4/mmm$	D_{4h}	-
Trigonal (Rhombohedral)	3	C_3	*+
	$\bar{3}$	$C_{3i}(S_6)$	-
	3m	C_{3v}	*+
	32	D_3	*
	$\bar{3}m$	D_{3d}	-
Hexagonal	6	C_6	*+
	$\bar{6}$	C_{3h}	*
	6mm	C_{6v}	*+
	6/m	C_{6h}	-
	622	D_6	*
Hexagonal	$\bar{6}m2$	D_{6h}	*
	$6/mmm$	D_{6h}	-
Cubic	23	T	*
	$\bar{4}3m$	T_d	*
	$m\bar{3}$	T_h	-
	432	O	-
	$m\bar{3}m$	O_h	-

the atomic arrangement at one end is different from the other opposite end. These crystals are called polar crystals and exhibit spontaneous polarization.

Polar crystals that have at least two equilibrium orientations for the spontaneous polarization vector in the absence of an external electric field and that can have their spontaneous polarization switched between these two equilibrium orientations by an applied external electric field are regarded as ferroelectric materials. The ferroelectric crystal is also defined as a dielectric material that has a net dipole moment even in the absence of an external electric field. This net dipole moment is due to the centre of the positive charge in the crystal not coinciding with the centre of the negative charge due to its crystalline structure, which is referred to as spontaneous polarization, P_s [10]. Based on the crystallographic point groups, all ferroelectrics are pyroelectric, and all pyroelectrics are piezoelectric, which generally belong to the dielectric. However, not all piezoelectrics are pyroelectric, and not all pyroelectrics are ferroelectric [23]. The relationship between ferroelectric, pyroelectric and piezoelectric together with their subgroups based on symmetry are summarized in Figure 2.

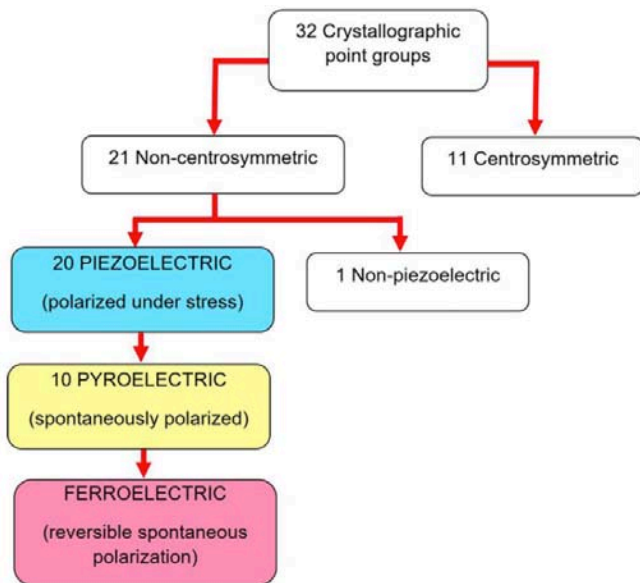


Figure 2: The interrelationship of ferroelectric and subgroups based on symmetry.

2.1. Ferroelectric Polymers and Nanofiller

Ferroelectric polymers and nanofillers are two different materials that can be combined to form composites with enhanced properties. Ferroelectric polymers are a type of polymers that have a ferroelectric effect, which implies that they have a spontaneous electrical polarization that can be reversed by an external electric field due to the asymmetric arrangement of the polymer's molecular dipoles. Nanofillers are low-dimensional particles or

nanoscale particles that can be dispersed in a polymer matrix to improve their properties. Metal nanoparticles, metal oxide nanoparticles, carbon-based materials (e.g., carbon nanotubes, graphene), and ceramics are examples of nanofillers. Nanofillers, when disseminated in a polymer matrix, can add new functionalities and improve the mechanical, electrical, and thermal properties of the composite.

2.1.1. Polyvinylidene Fluoride (PVDF) and Its Copolymer Polyvinylidene Trifluoroethylene P(VDF-TrFE)

Polyvinylidene fluoride (PVDF) and its copolymer with trifluoroethylene (TrFE) are ideal candidates for ferroelectric polymers because of their superior ferroelectric performance and ease of processing into thin films [24]. It was around 1970 when Kawaii discovered PVDF in the form of electret [25]. Poling the polymer PVDF with a high electric field induces orientation of the permanent dipoles and possibly creates a space charge by injection of free charge carriers between the electrodes to robust the electrical properties of a polymer. Soon after, Bergman reported the discovery of pyroelectricity and non-linear optical properties of PVDF in 1971 [26]. Lando and Doll proposed in 1968 that direct crystallization of polar PVDF can be induced by incorporating a small amount of trifluoroethylene (TrFE) and tetrafluoroethylene (TeFE) into PVDF from melt crystallization [27].

PVDF is a fluorocarbon polymer, which results from the polymerization of vinylidene fluoride (VDF) monomers with a chemical formula $(-\text{CH}_2-\text{CF}_2-)$. This $(-\text{CH}_2-\text{CF}_2-)$ monomer is built up from positively charged H-atoms and negatively charged F-atoms which are aligned in one direction and perpendicular to the chain axis (backbone). A dipole moment in PVDF perpendicular to the chain in each monomer originating from its high electronegativity of a fluorine atom and hydrogen atom and has a vacuum dipole moment of $\mu_v = 7 \times 10^{-30}$ Cm (2.1 Debyes). The dipole moment orientation is subjected to the conformation and packing of molecules as shown in Figure 3 for the polar unit, all-trans chain conformations and parallel packing of PVDF structure [28, 29]. Arrows indicate the dipole direction normal to carbon chains. If the molecule emerges as β phase (Form I) which has an all-trans (TTT) planar zigzag chain conformations (refer to Figure 3b) with a parallel packing (see Figure 3c), the dipoles are aligned in one direction, perpendicular to the carbon chain. β phase crystals arranged in a parallel packing, also known as a quasi-hexagonal-symmetry structure (Figure 3c), exhibit the greatest spontaneous polarization in the unit cell and are hence of particular importance for electrical properties. Higher spontaneous polarization, P_s

reflects greater ferroelectric behaviour which can be experimentally determined by D - E hysteresis measurements. The lattice constants of such a quasi-hexagonal-symmetry unit cell are $a = 0.850$ nm, $b = 0.491$ nm, and $c = 0.256$ nm [28, 29]. The sum of dipole moment over a unit volume, μ_v , yields a large crystalline polarization, P_s .

$$P_s = \frac{2\mu_v}{abc} = 130 \text{ mC/m}^2 \quad (1)$$

where a , b and c are the lattice constants with $a = 0.858$ nm, $b = 0.491$ nm and $c = 0.256$ nm, respectively. The dipoles in the β phase conformation are switchable by applying an electric field, thus the β phase is responsible for the PVDF's ferroelectricity [28].

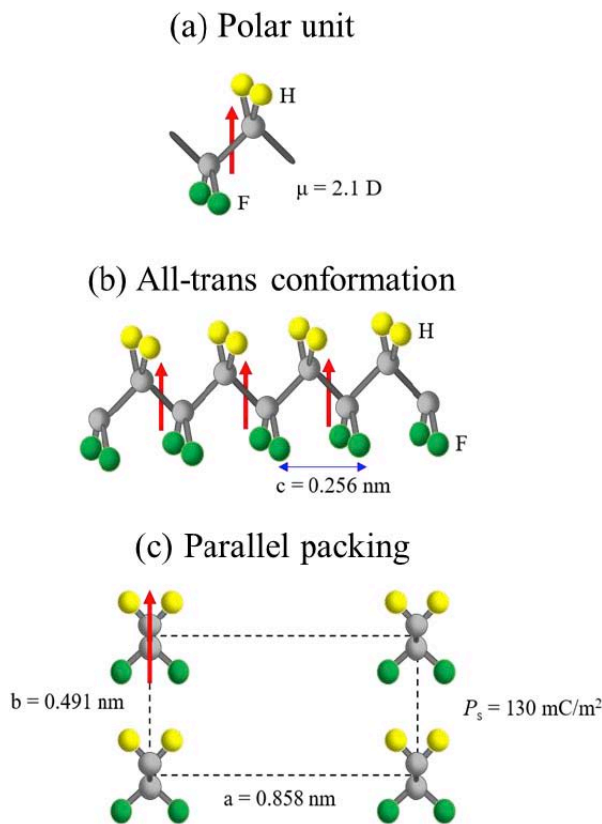


Figure 3: (a) unit, (b) molecule and (c) crystal structures of PVDF. Adapted from [28].

Ferroelectric behaviour observed in PVDF polymer is closely related to the alignment and orientation of its crystalline polymorph crystals. The thermal, mechanical and electrical treatments produce a specific crystalline polymorph of PVDF [30]. Melt-crystallization produces the α phase film as the most stable polymorph. P(VDF-TrFE) has been reported to crystallize into four types of crystalline phases which are β , α , γ and δ . P(VDF-TrFE) exhibits a much higher crystalline β phase compared to that of the pure PVDF and thus it tends to crystallize in the polar β phase by annealing at a temperature between the Curie transition temperature (T_c) and the melting temperature (T_m) without the need for mechanical

stretching [30, 31]. As P(VDF-TrFE) content is higher than 20 mol%, then it can directly be crystallized into the polar β phase [32]. Figure 4 shows the dipole orientation of monomer TrFE.

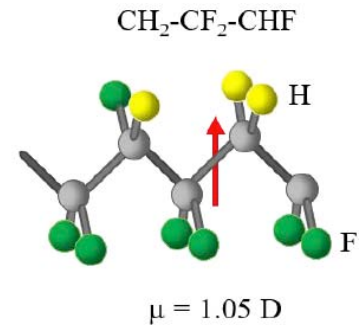


Figure 4: Dipole orientation of monomer TrFE.

The synthesis procedure of P(VDF-TrFE) films primarily for energy storage and energy harvesting applications involves several steps such as dispersing the P(VDF-TrFE) solution onto substrates using various techniques such as spin-coating [33, 34], dip-coating [35, 36], casting [37] and inkjet printing [38, 39], followed by film treatment and poling to enhance the ferroelectric properties. Films prepared with low evaporation rates and high boiling points solvents such as dimethylformamide (DMF), dimethyl sulfoxide (DMSO), and polar solvents such as diethyl carbonate (DEC) and methyl ethyl ketone (MEK) are favored for the formation of the polar phase PVDF. Annealing and poling treatments on P(VDF-TrFE) are former techniques to align polar domains in the films to increase their crystallinity. Mahdi *et al.* investigated the effect of annealing temperature on the crystalline structure of P(VDF-TrFE) (70/30) thin films using a hot plate with a wide range of annealing temperature (80 -140 °C) below and above the Curie temperature to optimize the crystalline structure [41]. The ferroelectric hysteresis analysis for film annealed at 100 °C demonstrates that the annealing treatment has the highest remnant polarization due to the highest percentage of crystallinity proven through XRD analysis. Even though spin-coating is a common method for thin film deposition, 2D and 3D printing processes such as screen printing and inkjet printing of polymer-based become a current need for device development for energy harvesting purposes. A review by Rodrigues-Marinho *et al.* reported that PVDF and its copolymer P(VDF-TrFE) were the most used polymers with barium-titanate as filler for piezoelectric nanogenerators fabricated by printing technologies [41].

2.1.2. Zinc Oxide Quantum Dots (ZnO QDs) Nanofiller

Because of their tunable physical dimensions and good optoelectronic capabilities due to size

confinement and anisotropic geometry, QDs have received a lot of attention as nanofillers. A quantum dot is a zero-dimensional relative to the bulk and the limited number of electrons results in discrete quantized energies in the density of states (DOS) for nonaggregate zero-dimensional structures. Semiconductor quantum dots with a particle size similar to that of the exciton Bohr radius has attracted significant attention to nanotechnology research nowadays because of their unique size-dependent optical and electronic properties. Among the II-VI binary compound semiconductors, ZnO QDs are of great importance due to their prominent features such as a wide direct energy gap of ~ 3.4 eV at room temperature, a large exciton binding energy of 60 meV and non-toxicity [42]. ZnO QDs are well known for their green, low-cost, simple and stable synthesis [43, 44] with excellent optical, electrical and electronic properties for a wide range of applications from optoelectronic to healthcare [45, 46]. An additional increase in the energy band gap leads to a smaller particle size of QDs. The extensive applications of ZnO QDs are attributed to their piezoelectricity, chemical stability and biocompatibility [47].

The crystal structures that emerged by ZnO are rock salt (or Rochelle salt), zinc blende and wurtzite as illustrated in Figure 5. The thermodynamically stable phase under ambient conditions is wurtzite symmetry. The wurtzite ZnO structure is composed of two interpenetrating hexagonal close-packed (hcp) sublattices and made up of alternating planes of Zn^{2+} and O^{2-} ions that are tetrahedrally coordinated along the threefold c -axis in fractional coordinates.

The wurtzite structure consists of a hexagonal unit cell with two lattice parameters $a = 3.25$ Å and $c = 5.21$ Å. This lattice type is classified by its point group 6mm (international notation) or C_{6v} (Schoenflies notation) and the space group C_{6v}^4 in the Schoenflies notation and $P6_3mc$ in the Hermann–Mauguin notation [49]. The space group $P6_3mc$ is non-centrosymmetric and is

allowed to exhibit ferroelectricity, although no polarization-electric field (D - E) loop has been observed until the melting point. Each zinc ion is surrounded by a tetrahedron of four oxygen ions and similarly, each oxygen ion is coordinated by a tetrahedron of four zinc ions. The arrangement of this tetrahedral coordination exhibits ZnO as a polar character, giving rise to spontaneous electric polarization, P_s [50]. ZnO QDs have distinguishable pyroelectric and piezoelectric properties due to the non-centre-symmetry in the wurtzite, which is used in piezoelectric sensors, mechanical actuators, and QD solar cells [51].

Several synthesis methods for preparing ZnO QDs, such as the sol-gel method, spray pyrolysis, precipitation, vapour phase transport process (VPT), thermal decomposition, hydrothermal synthesis and electrochemical growth. The sol-gel approach drew the most attention among these techniques due to its simplicity, low cost and scalability [52, 53]. There have been few reports on the use of quantum dots for pyroelectric applications. Recently, pyroelectric thin films with spherically symmetric PbS QDs that have an asymmetric ligand shell called Janus-ligand shell showed a pyroelectric coefficient, P_i of 1.97×10^{-7} C/m²K [54, 55]. Meanwhile, light-induced photodetectors based on the pyroelectric effect appear to be a current research trend [56-59]. An ultrafast self-powered CsPbBr₃ QDs photodetector based on light-induced pyroelectric effect has been demonstrated with a maximum pyroelectric current of 82.6 nA under the light intensity 98 mWcm⁻² [60]. However, these materials contain lead, which causes a major environmental impact. Exposure to environmental pollution should be avoided by using non-toxic or lead-free pyroelectric materials. ZnO nanorods (NRs) and nanowires (NWs) are well-known non-toxic materials for piezoelectric energy harvesting devices and are commonly synthesized by hydrothermal [61]. While ZnO nanorods have shown great promise for energy harvesting, it is important to note that their performance can be influenced by

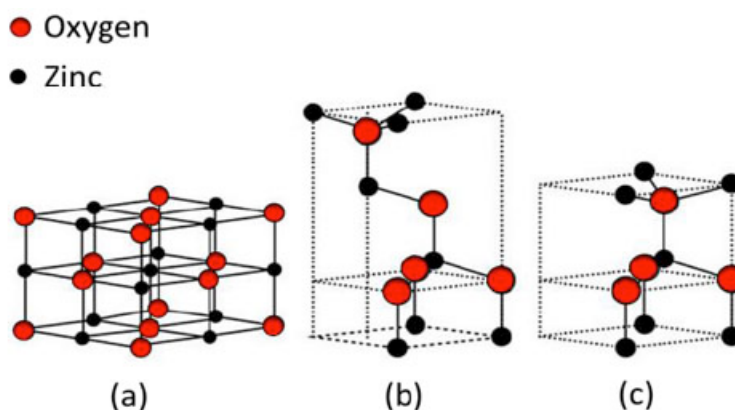


Figure 5: Zinc oxide crystal structure (a) cubic rock salt, (b) cubic zinc blende and (c) hexagonal wurtzite. Red and black colour indicate the oxygen and zinc atoms, respectively. Adapted from [48].

factors such as the dimensions of the nanorods, orientation, crystal structure and surface treatments and passivation [62-65]. The dimensions of the ZnO NRs or NWs, such as length, diameter and aspect ratio, can influence their pyroelectric response [66]. Li *et al.* reported that reducing the diameter size of the nanowires from 7 μm to 1.5 μm improved the piezoelectric coefficient from 18.2 to 46.9 pmV^{-1} [67, 61]. The increase of polarization per unit volume as the diameters of the NWs reduced is responsible for the improvement of the piezoelectric coefficient. By reducing surface defects, the stability and performance of ZnO NWs or NRs could be enhanced by surface treatments and passivation layers [68]. Recently, Rohul *et al.* were able to synthesize triethanolamine (TEA)-stabilized monodisperse ZnO QDs with an average size of 2.4 nm [69]. TEA ligands tend to encapsulate the surface of ZnO and hence lead to a smaller size of the QDs. Therefore, it is essential to investigate low-dimensional materials in pyroelectric energy harvesting, such as ZnO QDs, since they can contribute to enhancing the performance of functional devices in future research.

2.1.3. Ferroelectric Composites

Polymer composites comprising of ferroelectric particles embedded in polymer materials with different connectivity have generated great interest among known pyroelectric infrared detecting materials such as lead titanate (PT), lead zirconate titanate (PZT), barium titanate (BT) and triglycine sulfate (TGS) with poly-vinylidene fluoride (PVDF) or polyvinylidene fluoride-trifluoroethylene P(VDF-TrFE) as polymer host [70]. The properties of these composites depend on the following factors: (i) the properties of its constituents, (ii) the volume fraction of each constituent, (iii) the polarizability of particles and (iv) the nature of interconnecting these particles that make them promising materials for energy harvesting purposes [71]. As technology advances, ferroelectric composites are projected to play an important role in providing sustainable and environmentally friendly energy

sources for a wide range of electronic devices and sensors. Polyvinylidene fluoride (PVDF)-based triboelectric nanogenerators (TEGs) have been explored extensively as promising electric energy harvesting devices [72-74]. Recently, the fabricated PVDF-Ar.HBP-3/polyurethane (PU)-based TENG can power 12 LEDs without using a capacitor or rectifier when operating under a load and frequency of 10 N at 1 Hz. One of the reasons is due to the successfully improved polar β -phase of PVDF by the electrospinning approach, which is facilitated by the dipole interaction between the functional groups present in PVDF and Ar.HBP-G3 [75].

On the other hand, the introduction of zero-dimensional nanofiller into ferroelectric polymer hosts is of great interest nowadays to investigate the particle size's effect on their structural and physical properties. Nevertheless, the studies on the effect of embedding QDs into the ferroelectric polymer for energy storage and energy harvesting purposes are considered new due to the lack of reported works (as listed in Table 2). Table 2 remarks an electrical output of several composite films embedded with quantum dots filler. The filler aspect ratio, filler dispersion, filler alignment and orientation, polymer-polymer interaction, polymers and filler interaction, and the poling status are the key variables that determine the attributes of the ferroelectric nanocomposite. The extensive surface area of the filler may present benefits or limitations for such a system. The covalent bonding between the chains of capping ligands and the surface of quantum dots may lead to steric hindrance which can provide essential stability to the nanocomposite [76].

3. PROPERTIES OF MATERIALS FOR ENERGY HARVESTING

3.1. Dielectric Properties

There are two types of dielectrics which are polar and non-polar. The polar dielectrics have permanent dipole moments while the non-polar dielectrics do not possess any permanent dipole moment. Electric

Table 2: Ferroelectric Studies of Polymer Nanocomposite Films Embedded with QDs

Material	Method	Remark	Ref.
CdSe QDs/P(VDF-TrFE)	Langmuir-Blodgett	Exhibit approximately 6 μCm^{-2} for 60 nm composite films through <i>D-E</i> hysteresis loop	[77]
PMMA/carbon quantum dots (CDs)/PEDOT:PSS	Spin coating	Enlargement of the memory window with obvious I_{sc} and V_{oc} values in hysteretic I-V characteristic is due to the increment of dipole moment and spatial ordering in sandwiched multilayer which further increased the polarization electric field	[78]
CdSe/ZnS quantum dots/PVC	Solution casting	The lowest concentration of CdSe/ZnS in PVC (0.083 wt%) had the highest value of the dielectric constant compared with the concentration	[79]
$\text{Cd}_{1-x}\text{Zn}_x\text{Se}_{1-y}\text{S}_y$ nanodots/P(VDF-HFP)	Solution casting	Largest discharged energy density, $U_e \sim 26 \text{ Jcm}^{-3}$ among reported works so far in the polymer nanocomposites with low filler contents	[80]

polarization denotes an occurrence of the relative displacement of the negative and positive charges of atoms or molecules, the orientation of existing dipoles toward the direction of the field, or the separation of mobile charge carriers at the interfaces of impurities or other defect boundaries, caused by an external electric field [81]. The polarization (dipole moment per unit volume) of a dielectric material arises from four different mechanisms: i. Electronic polarization, ii. Ionic polarization, iii. Orientation dipolar polarization, iv. Space charge interfacial polarization or the Maxwell-Wagner effect.

The schematic structure of electrical polarization due to electrons, ions, dipoles and space charges with the applied field is illustrated in Figure 6. Electronic polarization originates from minor shifts in electron clouds from any atom within the dielectric corresponding to its positive nucleus. It is also occurring due to the polarization of localized electrons. Ionic polarization is caused by an electrical field that deforms the atomic nuclei arrangement or distortion of atomic position in a molecule or lattice. In the case of dipolar polarization, there is a tendency for permanent dipole to align by the electric field to give a net polarization in that direction. Space charge polarization can occur at the interface of metal to the dielectric, at grain boundaries in ceramics and at domain walls in ferroelectrics and is induced by migration charge carriers.

The total electric polarization of dielectric material is equal to the sum of electronic, ionic and orientation (if

there are some influences of impurities in the system) polarizations. The average polarization, \vec{P} has resulted from N amounts of electric dipole moments, \vec{p} which are all aligned per unit volume, V can be described by [84]:

$$\vec{P} = \frac{1}{V} \sum_{i=0}^N \vec{p}_i \tag{2}$$

where i is the number of dipole moments in the system.

Dielectric properties are generally denoted by a dielectric constant (represents polarization) and dielectric loss (represents relaxation). A dielectric relaxation phenomenon is observed in the orientation polarization or molecular fluctuation of dipoles due to the molecules. The dielectric relaxation phenomenon is due to the exponential decay of the polarization with time, with the removal of the external electric field in a dielectric substance. Meanwhile, a resonance effect is found in electronic or ionic polarization.

One of the important elements in dielectric spectroscopy is an investigation of the relaxation process of a material. Relaxation processes are due to rotational fluctuations of molecular dipoles and are characterized by a peak in the imaginary part, ϵ'' and a step-like decrease in the real part, ϵ' of the complex dielectric permittivity, ϵ^* increasing frequency, as shown in Figure 7 [84, 85]. Conversely, as the imaginary part of the dielectric function increases with decreasing frequency, hence conduction phenomenon can be observed. The real part of a complex dielectric function for pure ohmic conduction is independent of

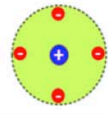
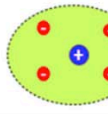
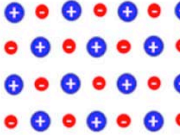
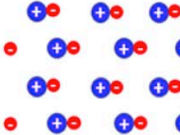
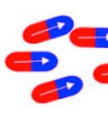
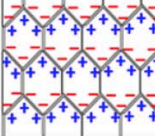
Polarization Mechanisms			
	Unpolarized state ($E = 0$)	Polarized state $\rightarrow E$	Originate
Electronic			polarization of localized electrons
Ionic			displacement of ions
Orientation Dipolar			reorientation of polar molecules
Space Charge Interfacial			long range of charge migration

Figure 6: Schematic illustrations of electronic, orientation, ionic and space charge polarization mechanisms. Adapted from [82, 83].

frequency while the imaginary part increases with decreasing frequency.

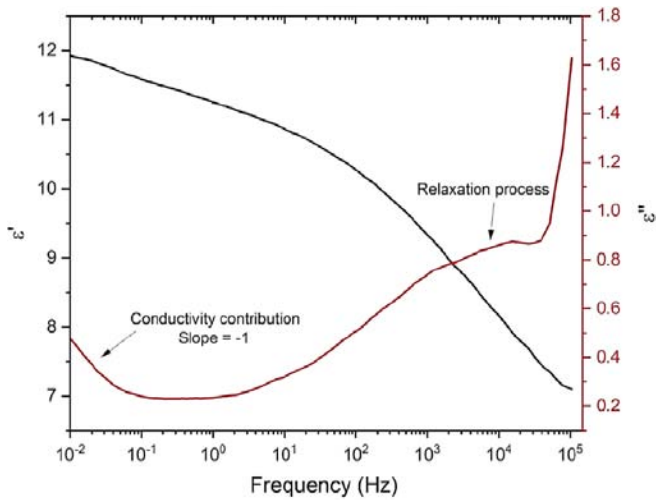


Figure 7: The real, ϵ' (black line) and imaginary, ϵ'' (red line) part of the complex dielectric function for a copolymer P(VDF-TrFE) 75/25 relaxation process at -20°C . Adapted from [86].

Many reports show that the annealing treatment of ferroelectric polymers such as PVDF and its copolymer P(VDF-TrFE) enhanced the degree of crystallinity and β crystalline domain of the materials and hence improved the dielectric, ferroelectric and pyroelectric properties. The study of annealed P(VDF-TrFE) by Mahdi *et al.* indicates that the optimized crystalline structure was achieved at around 100°C when the thin films were annealed with a hot plate and the morphology measurement by FESEM revealed the elongated rod-like crystallite structure as β crystalline phase (refer Figure 8b). Figure 8a illustrates the room temperature dielectric frequency spectra of

P(VDF-TrFE) treated with various annealing temperatures. The highest dielectric constant of P(VDF-TrFE) thin films $\epsilon' = 10.5$ when annealed at 100°C by using a hot plate [41]. The inclusion of fillers into a ferroelectric polymer to form composite materials could embark on the greater performance of energy-harvesting nanogenerators. PVDF with 7% MgO nanofiller showed the highest dielectric constant value $\epsilon' = 22$ compared to unfilled P(VDF-TrFE) as shown in Figure 9 [87]. This is due to the polarizability of PVDF upon application of the electric field, which is caused by an increase in polarized charges due to the dipolar contribution of the MgO nanofiller. Dielectric responses originating from the dipole-oriented polarization in the frequency range of 1 to 10^6 Hz play an important role in non-linear dielectric polymers. Fe-doped ZnO/P(VDF-TrFE) composite films reinforced the surface or interface polarization and resulted in a higher dielectric constant in composite films as compared to pure PVDF-TrFE films [88]. With the inclusion of Fe, in the presence of an external electric field, the freely moving charges in the conductive phases would be interrupted when passing through the resistance phases. This would result in a cloud of charge at the interface between the conducting phase and the resistive phase, which would manifest itself in increased polarization [88].

The effect of ZnO nanoparticles (NPs) in the PVDF matrix was studied in detail on unpoled and poled dielectric properties [89]. Tan *et al.* reported that the value ϵ' in the low-frequency region for 0.25 wt% PVDF/ZnO nanocomposite thin films increases faster than the value for PVDF thin films due to the presence

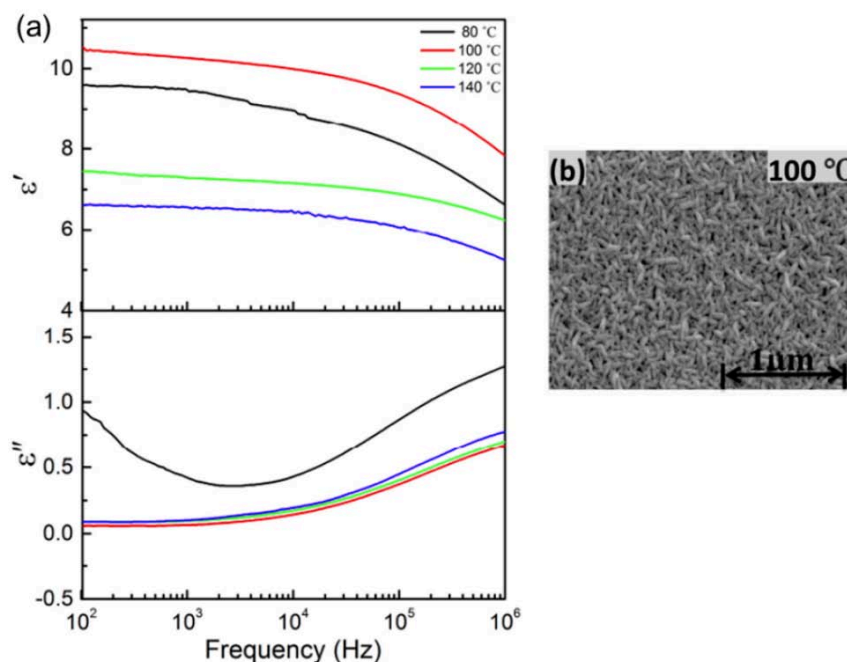


Figure 8: (a) Room temperature dielectric frequency spectra of P(VDF-TrFE) treated with various annealing temperatures (b) FESEM images of P(VDF-TrFE) annealed at 100°C [41].

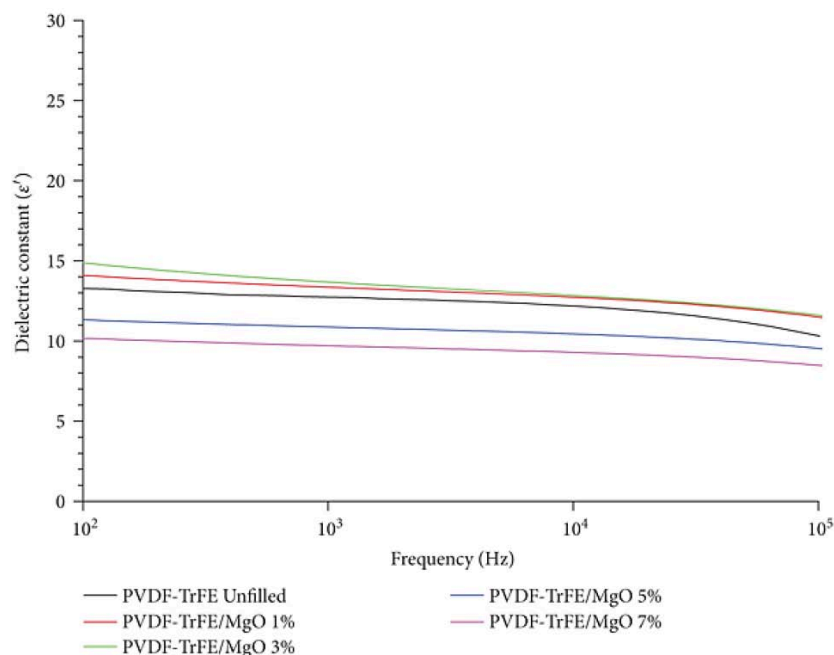


Figure 9: Dielectric constant versus frequency of PVDF-TrFE unfilled, PVDF-TrFE/MgO (1%), PVDF-TrFE/MgO (3%), PVDF-TrFE/MgO (5%), and PVDF-TrFE/MgO (7%) [87].

of ZnO nanoparticles after the poling process. This causes more charge carriers to be captured and as a result; the direct current conduction of the nanocomposite thin film has increased. Vo-Shi model [89, 90] fits well with the experimental data where $k = 65$ and $\varepsilon_2 = 2000$ give the best fit. The high k values indicate a strong interaction between the functional groups of the polymer and the surface of the nanoparticles. Since a smaller particle size has a larger fraction of interphase volume, this indicates a stronger polarization in the interphase surface. Therefore, the study concludes that the dielectric constant of the PVDF/ZnO nanocomposites can be increased tremendously although by doping with a very small amount and extremely small size of ZnO NPs.

Thus, the dielectric properties of materials are critical concerns in the design and application of nanogenerators. High-dielectric strength materials are preferred for industrial purposes to ensure that the nanogenerator can operate under various conditions without electrical breakdown.

3.2. Ferroelectric Properties

Ferroelectricity is a property of materials that have a spontaneous electric polarization that can be reversed by the application of an external electric field. A crystal is composed of a definite chemical composition in which the molecules are made up of positive ions and negative ions occupying lattice sites to constitute a crystal structure lattice. The smallest repeating unit of the lattice is called the unit cell and the specific symmetry of the unit cell identifies whether the crystal exhibits ferroelectric, piezoelectric, pyroelectric or

electro-optic effects [81]. Ferroelectric materials have received intensive investigation nowadays in exploring the uniqueness of their structural transformation phenomena. Generally, ferroelectric crystals possess one or more ferroelectric phases. The ferroelectric phase is a state that exhibits spontaneous polarization, P_s in a certain temperature range and the direction of the spontaneous polarization can be reoriented by an external electric field. Meanwhile, spontaneous polarization is defined by the value of the dipole moment per unit volume, or the value of the charge per unit area on the surface perpendicular to the axis of the spontaneous polarization or also referred to as the crystal axis. A spontaneous polarization can be written as:

$$P_s = \frac{\iiint \mu \, dV}{\text{volume}} \quad (3)$$

where μ is the dipole moment per unit volume. Ferroelectricity usually vanishes above a certain temperature called Curie or transition temperature, T_c . At the T_c , the crystal undergoes a phase transition from the polar state to the non-polar state. Above the transition temperature T_c , the crystal is said to be in the paraelectric state.

A ferroelectric crystal generally consists of regions called domains of homogeneous polarization, within each of which the polarization is in the same direction, but in the adjacent domains, the polarization is in different directions so that the net polarization of the specimen is equal to zero in the beginning when no electric field is applied. However, a strong field may reverse the spontaneous polarization of the domain

and this phenomenon is known as domain switching. Ferroelectrics are the most typical nonlinear dielectrics with switchable spontaneous polarization. The switching ability of the ferroelectric polarization can be observed by measuring the dielectric displacement current in response to a cyclic electric field which gives rise to a hysteresis loop (see Figure 10), the designation of ferroelectricity. At large signals, both the electric displacement, D and the polarization, P are nonlinear functions of the electric field, E was given as the linear equation below:

$$D = P + \varepsilon_0 E \quad (4)$$

where ε_0 is the permittivity of free space (8.85×10^{-12} C/Vm).

Applying a small amount of electric field on the ferroelectric crystal will exhibit only a linear relationship of P and E since the applied field is not enough to switch any domain or dipoles and the ferroelectric crystal will behave as a normal dielectric material (paraelectric). When the electric field is increasing, the dipoles begin to line up with the field (points 1 to 3 in Figure 10). Eventually, the field aligns all of the dipoles until all the domains are aligned in the positive direction and the maximum polarization is obtained. This state is the saturation state in which the crystal is composed of just a single domain. As the electric field strength decreases and reduces to zero, the polarization will generally decrease (at point 4) but does not return to zero, because some of the domains will remain aligned in the positive direction and the crystal will exhibit a remanent polarization, P_r . The ability to retain polarization permits the ferroelectric material to retain information, making the material useful in computer circuitry. The extrapolation of the linear line from point

3 back to the polarization axis (zero electric fields at point E) represents the value of the spontaneous polarization, P_s . When the electric field is applied in the opposite direction, the dipoles are reversed. A coercive field, E_c must be applied to remove the polarization and randomize the dipoles (point 5). Switching of ferroelectric polarization from one state to another can be achieved by applying an electric field higher than a threshold value, commonly known as the coercive field, E_c . It is also defined as the strength of the electric field required to reduce polarization to zero. Further increase of the electric field in the negative direction will cause saturation to occur in the opposite polarization (point 6). Thus, the cycle of the hysteresis loop can be completed by reversing the electric field direction once again.

As an electric field is applied to a ferroelectric crystal in an isothermal cycle, Joule heating disposes of the electrical flow to the system. The energy dissipated (W) per unit volume (V) of the ferroelectric crystal is equal to the area enclosed by the D - E schematic of the hysteresis loop which can be utilized for energy harvesting purposes [23]:

$$\frac{W}{V} = \int dDE \quad (5)$$

Due to the outstanding electrical properties close to the morphotropic phase boundary, lead-free ferroelectric ceramics have become a preferred choice for filler materials in ferroelectric nanocomposite [92-94]. Recently, the ternary BNT-BKT-BT-system included in P(VDF-TrFE) matrix results in higher ferroelectric and pyroelectric as compared to binary BNT-BT composition [92]. The value of remnant polarization, P_r was successfully increased by $\approx 65\%$

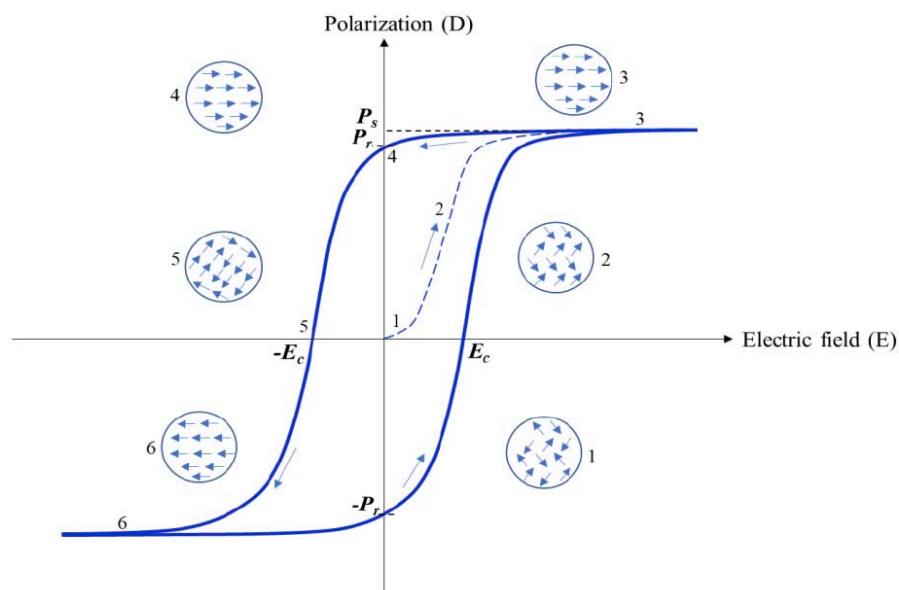


Figure 10: Typical P - E ferroelectric hysteresis loop. Circles with arrows represent the polarization state of the material at the indicated fields. Adapted from [91].

where P_r value increased from 85 mC/m² to 130 mC/m² when the volume fraction of BNT-BKT-BT increased from $\varnothing = 0$ to $\varnothing = 0.20$ as depicted in Figure 11a. The findings suggest that the increment of P_r is because of the enhanced polarization from dipole to dipole interaction of closely packed nanofiller as well as crack-free and defect-free composite formation in the polymer thin films [92, 95]. The discharged electric energy densities, U_e of P(VDF-TrFE)-BNT-BKT-BT nanocomposite films were integrated based on D - E hysteresis loop;

$$U_e = \int E dD \quad (6)$$

Figure 11b shows that the discharged U_e of 1.25 J/cm³ at 175 MV/m for the composite with $\varnothing = 0.20$ is 85% higher than that of the P(VDF-TrFE). The result indicates that the values of discharged energy density depend on the remnant of polarization of the D - E hysteresis loop [92]. Our previous work has successfully enhanced the ferroelectric properties of P(VDF-TrFE) with higher remnant polarization and discharged energy density by incorporating 0.15 wt% of ZnO QDs [96]. It is assumed that ZnO QDs filled in the P(VDF-TrFE) matrix locally induce additional dipole moments. These local dipoles coupled with polymer dipoles are speculated to cause an increase in ferroelectricity [96]. Meanwhile, one-dimensional (1D) multiferroic BiFeO₃ and P(VDF-TrFE) exhibited a saturated hysteresis loop with the highest remnant polarization, $P_r = 9.7$ mC/m² at 2 MV/m for BFO-50 vol % [97]. BFO fillers in the composite enhanced the remnant polarization due to the larger polarization nature of BFO as compared to PVDF. The higher remnant polarization in PVDF/BFO composites can be attributed to the enhanced polarization due to the dipole-dipole interaction of closely packed powders. Thus, ferroelectric materials, especially related to pyroelectric nanogenerators (PNGs) have promising applications and implications for various industries.

3.3. Pyroelectric Properties

The pyroelectric effect was first discovered in tourmaline by Teophrast [98]. Pyroelectric materials are dielectric materials that possess spontaneous electrical polarization and appear even in the absence of an applied electrical field or stress. All ferroelectric materials exhibit pyroelectricity but not all pyroelectric materials exhibit ferroelectricity. The pyroelectricity of a material is measured by the pyroelectric coefficient, P_i . A small change in temperature, ΔT in the crystal, results in a change in the spontaneous polarization vector, ΔP_s and can be written as:

$$\Delta P_s = P_i \Delta T \quad (7)$$

The pyroelectric coefficient, P_i is a vector with three components and describes the change in the electrical charge per unit surface area during heating or cooling. The unit of a pyroelectric coefficient is represented by C/m²K or $\mu\text{C}/\text{m}^2\text{K}$ [99]. In general, a homogeneous pyroelectric material with a constant pyroelectric coefficient throughout the temperature at any time is uniform, and the electric current generated from the pyroelectric effect is expressed as [100]:

$$i_p = \frac{dQ}{dt} = P_i A \frac{dT}{dt} \quad (8)$$

where the equation above denotes pyroelectric charge (Q), pyroelectric current (i_p), rate of temperature change (dT/dt), the surface area of the pyroelectric material (A) and pyroelectric coefficient (P_i).

Based on the thermodynamic diagram in Figure 12 illustrates the thermodynamically reversible interactions that may occur among the thermal, mechanical, and electrical properties of a crystal [101]. Variables S , D , and ϵ in the inner circles denote entropy, dielectric displacement, and strain, respectively. Pyroelectricity is a coupled effect where a change in temperature causes a change in electric displacement,

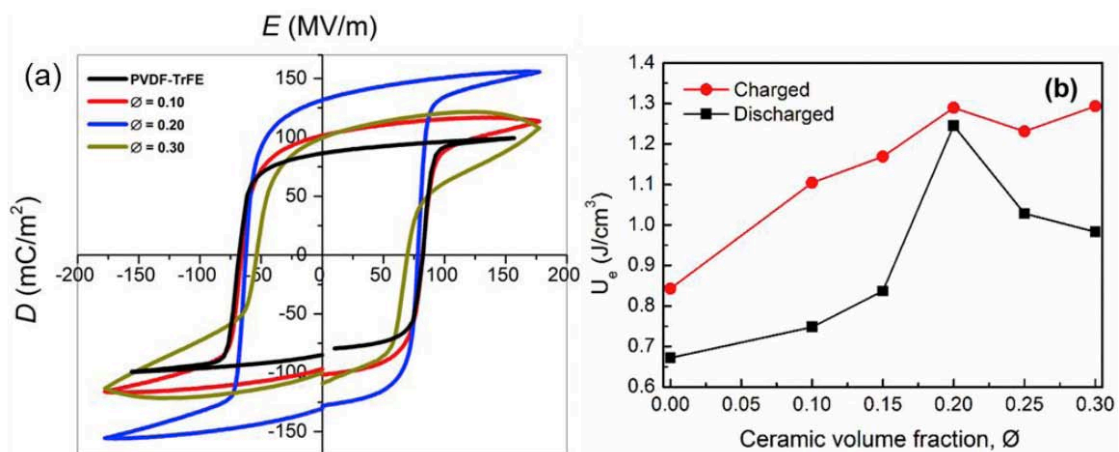


Figure 11: (a) D - E hysteresis loops (b) Charged and discharged energy densities, of pure P(VDF-TrFE) and P(VDF-TrFE) nanocomposite thin films as a function of ceramic volume fraction, \varnothing [92].

D (C/m^2). There are two routes to the pyroelectric effect. The primary route is shown by a solid red line and the second route is indicated by a dotted red line. In the first route, the primary pyroelectric effect is caused by a change in temperature, which leads to a change in the electric displacement in a crystal under constant strain σ , rigidly clamped to prevent expansion or contraction (in other words, the shape and size of a crystal held fixed during heating). The primary pyroelectric effect signifies a direct coupling between polarization and temperature. In the second route, the secondary pyroelectric effect is a result of crystal deformation which means that the crystal may be in free form, thus the thermal expansion occurs freely. The total pyroelectric coefficient mechanically free condition is given as [102]:

$$p^{\sigma,E} = p^{\varepsilon,E} + d_{ij}e_{ij}^E\lambda_i^E \quad (9)$$

where the first term on the right-hand side of the equation shows the primary pyroelectric coefficient under constant strain conditions while the second term represents the secondary pyroelectric coefficient, which tensors d_{ij} , e_{ij}^E and λ_i^E are the piezoelectric coefficient, elastic constant and thermal expansion coefficient, respectively.

Another pyroelectric effect obtained from the pyroelectricity arises from the path $T \rightarrow \varepsilon \rightarrow D$ as shown in Figure 12. As a result, when the crystal is free to deform or expand, an electrical displacement, D obtained from thermal expansion. This causes a strain ($T \rightarrow \varepsilon$), which in turn by the piezoelectric path ($\varepsilon \rightarrow D$) contributes to the electrical displacement, D . This is called the pseudo pyroelectric effect or false pyroelectric of the first kind. Temperature changes in lattice constant are related to the changes of elementary dipole moments, consequently resulting in polarization [103].

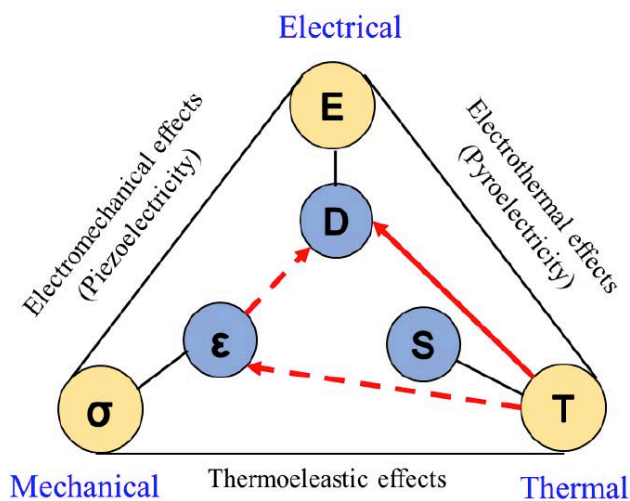


Figure 12: The relationships between the thermal (temperature), mechanical (strain) and electrical (field) properties of a crystal. Adapted from [101].

A typical temperature and pyroelectric current wave profile versus time obtained during the heating and cooling of the pyroelectric sample at a linear rate is shown in Figure 13. The rate of temperature change is calculated from the gradient of the triangular wave of the sample temperature, while the pyroelectric current can be obtained from the amplitude of the square wave profile [104].

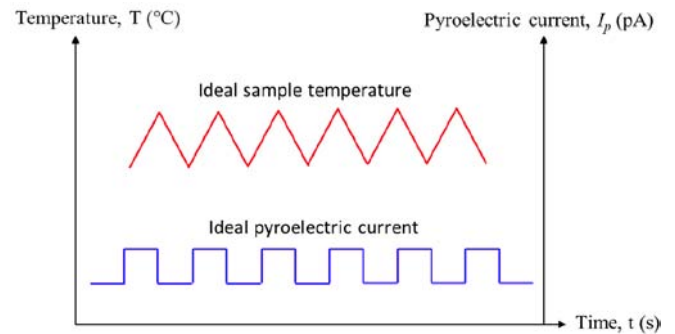


Figure 13: Ideal rectangular short-circuited pyroelectric current spectra in response to triangular temperature wave. Adapted from [105].

Pyroelectric properties of polymer and nanocomposite materials such as pyroelectric coefficient (P_i), dielectric constant (ε'), detectivity (F_D) and energy harvesting (F_E) of the figure of merit and discharged electric energy densities (U_e) with -PVDF as polymer host are listed in Table 3. The composite film of P(VDF-TrFE)-BNT-BKT-BT [106] shows the highest pyroelectric coefficient and significant performance of F_D among all reported works in Table 3. Although ceramic fillers like BNT exhibit high pyroelectric properties as indicated in Table 3, it is essential to study quantum size effects like ZnO QDs on the electrical (ferroelectric, dielectric and pyroelectric) performance of energy harvesting and storage devices. Our previous work [96] shows that 0.15 wt% of ZnO QDs in P(VDF-TrFE) could contribute about half of the pyroelectric coefficient reported by [96] with a QDs size in the range of $\sim 2.5 - 3$ nm. The interfacial polarization may arise from the interaction between the nanofiller and the polymer matrix during the poling process and contribute to the increase in the remnant polarization and pyroelectric coefficient achieved in this work. The surface morphology of P(VDF-TrFE) with ZnO QDs fillers shows the distribution of spherically shaped crystalline micelles embedded inside the elongated rod-like structures as shown in Figure 14a. Among all the variants of films embedded with ZnO QDs, 0.15 wt% films had the longest average length of elongated rod-like shape. As a result, the polarization of the nanocomposite films, which contributes to the ferroelectric performance, depends proportionally on the length of the elongated rod-shaped structure of P(VDF-TrFE) [106]. The figure of merit (FOM), F_E is an indicator for assessing the

energy harvesting performance of the pyroelectric device, expressed by equation (10) [107];

$$F_E = \frac{P_i^2}{\epsilon_0 \epsilon_r} \quad (10)$$

where ϵ_0 is the permittivity of free space ($8.854 \times 10^{-12} \text{ Fm}^{-1}$) and ϵ_r is the permittivity of the pyroelectric material. The maximum F_E calculated at 1 kHz is $19.5 \text{ Jm}^{-3}\text{K}^2$, for 0.15 wt% P(VDF-TrFE)/ZnO QD composite film as depicted in Figure 14b. Therefore, the addition of ZnO QDs improved the energy harvesting performance of nanocomposite devices substantially. Another type of FOM is the detectivity without division of the specific heat capacity, F_D [108], which is normally used for thermal sensors. The expression is stated as:

$$F_D = \frac{P_i}{\sqrt{\epsilon' \tan \delta}} \quad (11)$$

where P_i , ϵ' and $\tan \delta$ are the pyroelectric coefficient, dielectric constant and tangent loss, respectively.

Figure 14b shows that F_D reaches a maximum of $93 \text{ C/m}^2\text{K}$ at 0.15 wt% ZnO QDs. This study indicates that a device made with P(VDF-TrFE)/ZnO QDs showed good functionality for energy harvesting and thermal sensing with less than 1% ZnO QDs in the P(VDF-TrFE) copolymer. Thus, it is believed that varying the quantum dots' size may open the possibility to control the pyroelectric properties of polymer nanocomposites. Hence, in the future, the investigation of the quantum size effect of ZnO QDs in different size ranges on P(VDF-TrFE) is necessary to explore their potential ferroelectric, dielectric and pyroelectric properties.

Wearable electronic devices based on PNGs onto the human body is one of the current interests among researchers. A few factors need to be considered such as flexibility, stretchability, or fibrous materials, in order to use PNGs as wearable devices [111]. Xue *et al.* reported integrated a N95 respirator and a PVDF thin film PNGs for harvesting energy of human respiration

Table 3: Pyroelectric Properties of ZnO, QDs and Nanocomposite Polymer Films

Material	Ø or wt%	P_i ($\mu\text{Cm}^{-2}\text{K}^{-1}$)	ϵ'	F_D ($\mu\text{Cm}^{-2}\text{K}^{-1}$)	F_E (Jm^{-3}K^2)	U_E (Jcm^{-3})	Ref.
ZnO NW	-	12	-	-	-	-	[109]
ZnO bulk	-	9.4	-	-	-	-	[101]
PbS QDs	-	0.197	-	-	-	-	[54]
PVDF/ La_2O_3	3.0 wt%	42	~8	86	-	-	[108]
P(VDF-TrFE)-BNT-BKT-BT	Ø = 0.20	95	~20	137.99	-	-	[106]
PVDF/ ZnO NRs	-	-	-	-	-	P_r = $0.2188 \mu\text{C/m}^2$	[110]
PVDF/ZnO NPs	0.25 wt%	29	15	-	-	-	[89]
P(VDF-TrFE)/ZnO QDs	0.15 wt%	49	13.9	93	19.5	1.18 $P_r = 10.02 \mu\text{Cm}^{-2}$	[96]

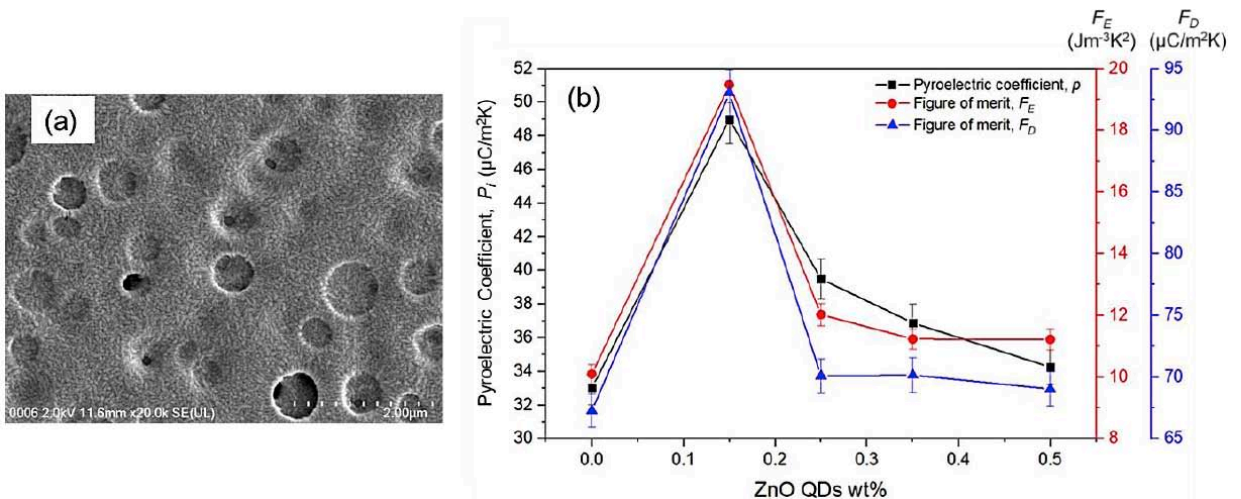


Figure 14: (a) FESEM images of 0.15 wt% of P(VDF-TrFE)/ZnO QD films annealed at $100 \text{ }^\circ\text{C}$, **(b)** Pyroelectric coefficient and energy harvesting and detectivity figure of merit (F_E and F_D) against ZnO QDs variations [96].

[111, 112]. Self-powered breathing sensor was demonstrated using a flexible PVDF film installed on a common respirator for sustainable energy harvesting and self-powered breathing monitoring. The 30 μm PVDF thin film was exposed by the body exhaled gas that had the same temperature of the body. The temperature-changing rate of the PNGs by human exhaled gas was $13\text{ }^\circ\text{Cs}^{-1}$ and the corresponding peak output current and voltage of the PNGs was $2.5\text{ }\mu\text{A}$ and 42 V , respectively. The maximum output performance of the PNGs was $8.31\text{ }\mu\text{W}$ at the load resistance of $50\text{ M}\Omega$ and the PNGs showed stable output performance after ten days without power degradation [111, 112]. Therefore, the development of pyroelectric nanogenerators is proven to be crucial for the commercialization of electronic devices as they provide a renewable and self-sufficient energy source.

3.4. Thermally Stimulated Current (TSC)

Thermally stimulated current, TSC measurement is extensively studied in diverse fields, i.e., physics, electronics, electrical engineering, chemistry, ceramics and biology. TSC is a method to investigate the molecular relaxations phenomena of dielectric and semiconducting materials which are generally involving the study of thermally activated charge, electron trap and activation energy of a material. TSC operates as short-circuit current that flows during heating due to the displacement of positive and negative charges (e.g., electrons, holes, ions) as well as to the rotational motion of permanent dipoles in samples, due to the phase transition of materials (e.g., the glass polarization phase, Curie point, etc.) [113].

TSC measurement involves the emergence of temporal thermoelectrets. An electret is defined as a piece of dielectric material having quasi-permanent electrical charges. There are various ways to form electrets in a dielectric material either by the application of an electric field between metallic electrodes, or by the application of a strong static magnetic field, or simply by a thermal process without both fields and also by the application of mechanical pressure to the dielectric material. The sources of electrets are commonly from both dipole polarization and space charges. These kinds of charges can be trapped within

the materials or with time they may form layers of surface charges (see Figure 15). An electret also could be formed as a carrier that is transferred in a molecular or domain structure throughout the dielectric. The trapped positive and negative carriers may be formed as layers of space charges which are often positioned close to the two surfaces of the electrets [114].

Reliable mechanisms for TSC include several processes that contribute to the discharge of electrets, where restoration of charge neutrality is essentially a driving force for all the processes. These processes can be classified into two main categories [114-116]:

1. Disorientation of Dipoles

By redistributing all dipoles at random, this technique tends to eradicate persistent dipole polarization. It entails the rotation of a couple of positive and negative charges, which necessitates the expenditure of a specific quantity of energy known as activation energy. It could be a few eV per dipole in a solid dielectric. Dipole disorientation is thus a thermally induced phenomenon that can be increased by heating. The activation energy of each dipole in electrets is generally different from one another. As a result, as illustrated in Figure 16, current–temperature plots reveal several relaxation peaks. At low temperatures, dipoles with low activation energy will disorient. Those polarized dipoles with high activation energy, on the other hand, will disorient at a higher temperature. The peaks associated with dipoles include the following:

(a) γ and β Peaks

The disorientation of dipoles at low temperatures is represented by these peaks. Individual peaks might overlap and merge into a broad peak due to small changes in activation energy. B peak is a term used in polymers to describe a broad peak. Depolarization activities by polar side groups with continuous distribution activation energies is attributed to this peak.

(b) α Peak

This is another broad peak that has formed because of overlapping peaks. The origin, on the other hand, identifies this relaxation peak, with small variations in

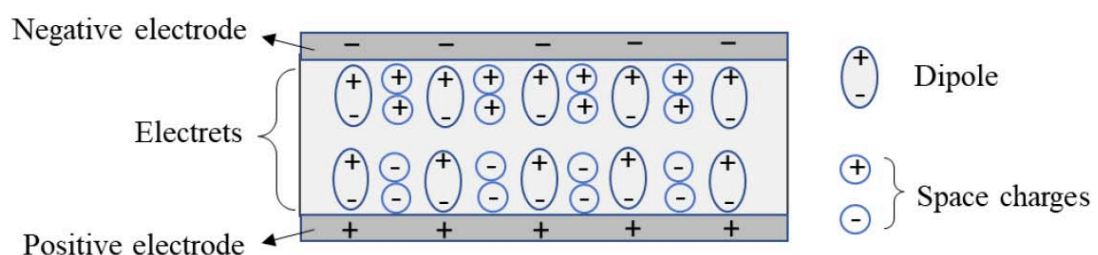


Figure 15: Schematic configuration of typical electrets with aligned dipoles and space charges. Adapted from [115].

dipole rotational mass causing the peak to arise. When polymers are heated to their softening temperature, for example. The mobility of major chain segments within the polymers causes the dipoles to become disoriented. The α peak in Figure 16 is produced by disorientation by various dipoles, and it is positioned at the glass-rubber transition temperatures T_g of the polymers.

2. Space Charges – ρ Peak

In electrets, immobilized space charges are stored in a non-uniform manner and are frequently seen around electrodes. The heating process, on the other hand, gives energy to these carriers, allowing them to migrate and neutralize at the electrodes and within the electrets. The recombination of charges with opposite signs is involved in these neutralization processes. The drift in the local electric field and diffusion, which tends to remove the charge concentration gradient, are the driving forces. The emergence of ρ peaks in Figure 16 characterizes this relaxation effect. When compared to the temperatures of β and α peaks, it appears at a higher temperature. This is because dipole disorientation only requires local rotation. The neutralization of space charges, on the other hand, necessitates their transit over many atomic distances. As a result, space charges should have sufficient energy to operate at a higher temperature.

There are limited recent studies based on the TSC of ferroelectric polymer P(VDF-TrFE) and its composite. However, it is crucial to discuss the relaxation behaviour during the phase transition of copolymers, especially at a glass transition and Curie temperature, as well as the effect of nanofillers on these two relaxation peaks. In 2013, TSC study of P(VDF-TrFE) copolymer by Capsal *et al.* showed two relaxations spectra, α and ρ (Curie mode) which are centered around $T_{\alpha} = -24$ °C and $T_{\rho} = 103$ °C, respectively [118]. The α mode is attributed to the dielectric manifestation of the glass transition. The activation enthalpies for relaxation are given in the range from 100 kJ/mol to 280 kJ/mol. The relaxation associated with the Curie

transition has been assigned to dipolar reorientations in the crystalline phase of these semi-crystalline polymers. Activation enthalpies of the Curie relaxation are higher than for the α mode.

Our previous study on TSC of annealed P(VDF-TrFE) revealed three depolarization peaks which are β , α and ρ [119]. The low intensity β peak emerges at a lower temperature region of -75.5 °C, which is associated with the relaxation of the side chains on the polymer backbone in the amorphous phase [120]. The data fitting for the first-order kinetic theory [121] known as the decomposition or deconvolution technique is used to determine the type of relaxation processes that participated in the formation of the TSC peaks, as well as the activation energies involved in each of the relaxation peaks. Decomposition analysis can reveal some well-known relaxation phenomena such as space charge (Curie mode, ρ) (0.85 eV, 1.1 eV) [122], segmental relaxations (T_g peak) (1.0 – 2.9 eV) [118, 123] and dipole group (β peak) (0.18 eV, 1.17 eV) [124, 116] with their respective activation energies. The respective values of activation energy are referred for PVDF and its copolymer P(VDF-TrFE) as reported by others. Dipoles with low activation energies will disorient at low temperatures, while polarized dipoles with high activation energies will disorient at relatively high temperatures. The study demonstrates that the dipoles of the annealed P(VDF-TrFE) film with a frozen backbone chain have low activation energies of approximately 0.3 eV to 4.1 eV as depicted in Figure 17a. These values correspond to the energy needed for localized polarization of the copolymer side chains. As the TSC heating process crosses their $T_g(\alpha_1)$, the segmental molecules receive enough thermal energy to assist the mobility of polarized and frozen main chains to depolarize and then randomize. This process involves the motion of about 40 to 50 carbon atoms on polymer backbones. The relaxation mode of α_1 as shown in Figure 17b can be fitted by three decomposed peaks with activation energies in the range of 2.4 to 9.8 eV. Further heating above T_g

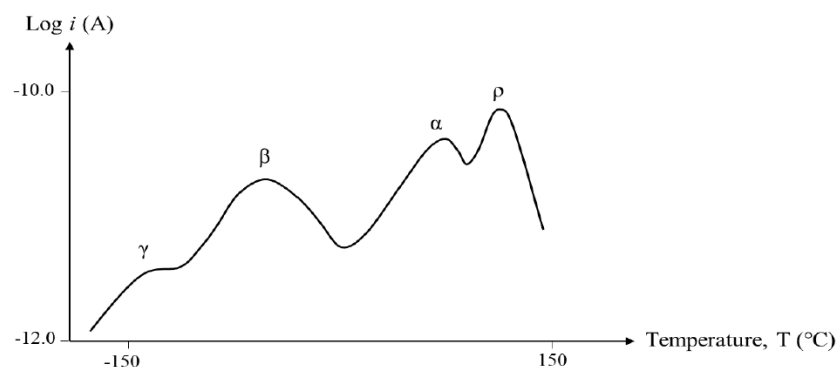
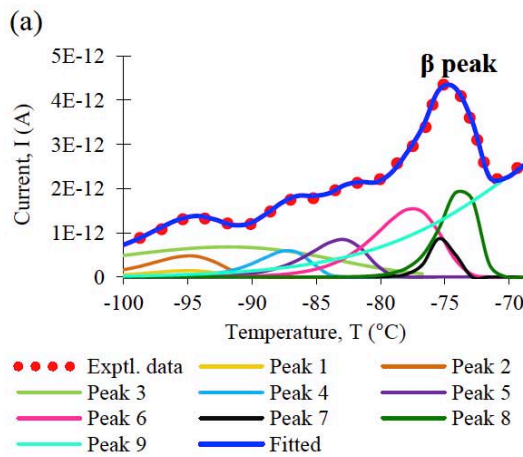
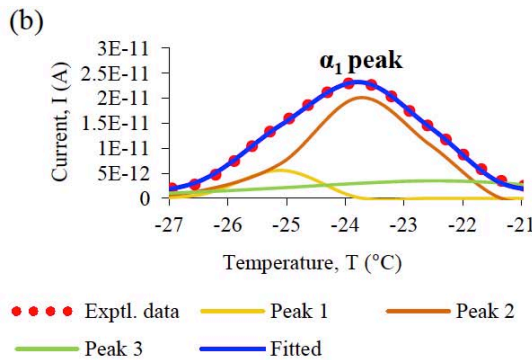


Figure 16: Schematic illustration of typical TSC result for PMMA. The symbols γ , β , α and ρ indicate relaxation peaks in the material. Adapted from [117].



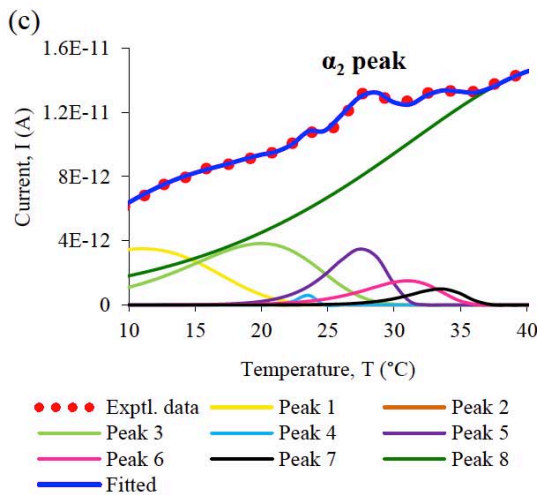
Peak	T_{max} (°C) ± 0.01	I_{max} (A) ± 0.01	E_{fit} (eV)
1	-95	1.45E-13	1
2	-94.9	4.80E-13	1
3	-92	6.80E-13	0.3
4	-87.2	6.00E-13	1.5
5	-83	8.50E-13	1.4
6	-77.5	1.55E-12	1.3
7	-75	1.00E-12	4.1
8	-73.6	2.07E-12	2.5
9	-63	3.10E-12	0.5
β	-74.2*	4.28E-12*	

*measured



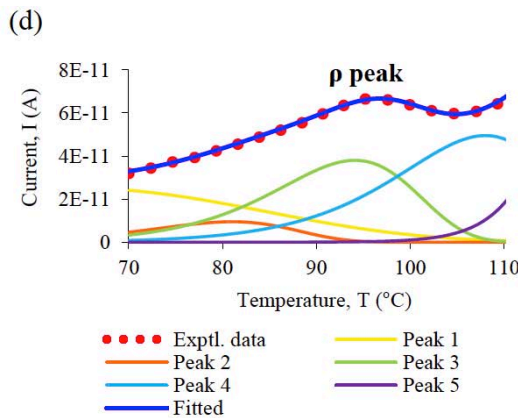
Peak	T_{max} (°C) ± 0.01	I_{max} (A) ± 0.01	E_{fit} (eV)
1	-22.4	3.50E-12	2.4
2	-23.4	2.18E-11	6.3
3	-24.8	6.30E-12	9.8
α₁	-23.77*	2.32E-11*	

*measured



Peak	T_{max} (°C) ± 0.01	I_{max} (A) ± 0.01	E_{fit} (eV)
1	11	3.50E-12	1.1
2	19.5	1.00E-13	8
3	20	4.00E-12	1.5
4	23.5	6.00E-13	12
5	27.6	3.50E-12	3.7
6	31	1.60E-12	2.9
7	33.5	1.00E-12	4
8	43	1.50E-11	0.7
α₂	28.66*	1.32E-11*	

*measured



Peak	T_{max} (°C) ± 0.01	I_{max} (A) ± 0.01	E_{fit} (eV)
1	62	2.55E-11	0.4
2	81	9.50E-12	1.4
3	94.1	3.80E-11	1.52
4	108	4.95E-11	1.5
5	121	1.48E-10	3.6
ρ	96.34*	6.68E-11*	

*measured

Figure 17: Decomposition of the TSC spectrum of the annealed P(VDF-TrFE) at 100 °C for β , α_1 , α_2 and ρ relaxation peaks. Adapted from [119].

reveals a second relaxation peak, α_2 , as shown in Figure 17c, but with a very low intensity and energy of

approximately 0.7 to 8 eV. According to Teyssendre et al., this peak represents the molecular mobility of

amorphous domains constrained by crystallites [126]. The Curie mode ρ peak associated with the molecular motion of the polarized dipole moments, together with the injected space charge, is shown in Figure 17d. The maximum calculated activation energy for the ρ peak is 3.6 eV. The findings state that all the relaxation modes of β , α_1 , α_2 and ρ can be associated with deep traps due to the highly polar molecular structure of P(VDF-TrFE) and trapping of charge carriers on the surface region of the copolymer [119].

Understanding TSC behavior in nanomaterials can be valuable for materials development. TSC can be used to identify charge carrier mobility, which is a crucial factor in semiconductor manufacturing. TSC can help enhance the electrical characteristics of materials used in optoelectronic devices such as LEDs and photodetectors, boosting their performance and reliability [127, 128].

4. CONCLUSION

The basic properties of nanogenerator materials such as ferroelectric, dielectric, pyroelectric and Thermally Stimulated Current are reviewed. PVDF and its copolymers P(VDF-TrFE) are the most suitable candidates for polymer hosts in the fabrication of polymer nanocomposite devices due to the high pyroelectric coefficient, which is contributed by their oriented molecular dipoles. The ferroelectric and pyroelectric properties of copolymer thin films P(VDF-TrFE) that employed in sensor and energy harvesting applications are influenced by crystallinity, surface morphology, molecular chain orientation, and polarization. Furthermore, QDs such as ZnO have shown good potential for biocompatible nanogenerators and can be used as a nanofiller in P(VDF-TrFE) polymer host. The inclusion of non-centrosymmetric nanocrystal ZnO as fillers into the copolymer matrix may increase the polarization of the polymer nanocomposite due to the dipole-dipole interaction of closely packed nanoparticles and interfacial polarization and consequently increase the current generated from pyroelectric activities. A significant improvement in ferroelectric and dielectric properties can also be observed as a result of synergistic interactions between the QDs with the polymer host. The quantum size effect of ZnO QDs on the energy harvesting capability of this polymer nanocomposite can be further explored and investigated to obtain optimized performance. It is crucial to investigate the particle size effect (at different size ranges) of ZnO QDs in P(VDF-TrFE) to discover the highest functional properties as energy harvester nanogenerator. Although PVDF-based polymers have high biocompatibility and are promising candidates, as wearable or even implantable electronics, the security

of devices is the most important factor. The compatibility and user-friendliness of the devices must also be considered in the manufacturing process. With new materials, new structures and new methods being successively applied to the design of PVDF-based nanogenerators, thereby driving the commercial application of a new self-driven sensing and energy harvester is hopefully reliable and sustainable in the future.

DECLARATION OF COMPETING INTEREST

The authors declare no conflict of interest.

ACKNOWLEDGEMENT

The authors are grateful for the financial support from the Ministry of Higher Education Malaysia under the Fundamental Research Grant Scheme (FRGS/1/2019/STG02/UM/01/2), the Universiti Malaya Impact-Oriented Interdisciplinary Research Grant Program, Project No. IIRG007B-19FNW.

REFERENCES

- [1] Xue H, Yang Q, Wang D, *et al.* A wearable pyroelectric nanogenerator and self-powered breathing sensor. *Nano Energy* 2017; 147-54. <https://doi.org/10.1016/j.nanoen.2017.05.056>
- [2] Ryu H, Kim SW. Emerging pyroelectric nanogenerators to convert thermal energy into electrical energy. *Small* 2021; 1903469. <https://doi.org/10.1002/sml.201903469>
- [3] Zhao X, Askari H, Chen J. Nanogenerators for smart cities in the era of 5G and Internet of Things. *Joule* 2021; 5(6): 1391-431. <https://doi.org/10.1016/j.joule.2021.03.013>
- [4] Pang Y, Cao Y, Derakhshani M, Fang Y, Wang ZL, Cao C. Hybrid energy-harvesting systems based on triboelectric nanogenerators. *Matter* 2021; 4(1): 116-43. <https://doi.org/10.1016/j.matt.2020.10.018>
- [5] Kim Y, Wu X, Lee C, Oh JH. Characterization of PI/PVDF-TrFE composite nanofiber-based triboelectric nanogenerators depending on the type of the electrospinning system. *ACS Appl Mater Interfaces* 2021; 13(31): 36967-75. <https://doi.org/10.1021/acsami.1c04450>
- [6] Dai Y, Zhong X, Xu T, Li Y, Xiong Y, Zhang S. High-performance triboelectric nanogenerator based on electrospun PVDF-Graphene Oxide nanosheet composite nanofibers. *Nano Energy* 2021; 11(9): 2300426. <https://doi.org/10.1002/ente.202300426>
- [7] Ong DT, Koay JS, Sim MT, *et al.* High performance composition-tailored PVDF triboelectric nanogenerator enabled by low temperature-induced phase transition. *Nano Energy* 2023; 113: 108555. <https://doi.org/10.1016/j.nanoen.2023.108555>
- [8] Cai C, Luo B, Liu Y, *et al.* Advanced triboelectric materials for liquid energy harvesting and emerging application. *Mater Today* 2022; 52: 299-326. <https://doi.org/10.1016/j.mattod.2021.10.034>
- [9] Choi YS, Kim SW, Kar-Narayan S. Materials-related strategies for highly efficient triboelectric energy generators. *Adv Energy Mater* 2021; 11(7): 2003802. <https://doi.org/10.1002/aenm.202003802>
- [10] Nguyen QH, Ta QT, Tran N. Review on the transformation of biomechanical energy to green energy using triboelectric and

- piezoelectric based smart materials. *J Clean Prod* 2022; 133702.
<https://doi.org/10.1016/j.jclepro.2022.133702>
- [11] Delgado-Alvarado E, Elvira-Hernández EA, Hernández-Hernández J, Huerta-Chua J, Vázquez-Leal H, Martínez-Castillo J, García-Ramírez PJ, Herrera-May AL. Recent progress of nanogenerators for green energy harvesting: Performance, applications, and challenges. *Nanomaterials* 2022; 12(15): 2549.
<https://doi.org/10.3390/nano12152549>
- [12] Divya S, Oh TH, Bodaghi M. 1D Nanomaterial Based Piezoelectric Nanogenerators for Self-Powered Biocompatible Energy Harvesters. *European Polymer Journal* 2023; 112363.
<https://doi.org/10.1016/j.eurpolymj.2023.112363>
- [13] Wang YM, Zeng Q, He L, et al. Fabrication and application of biocompatible nanogenerators. *Iscience* 2021; 24(4).
<https://doi.org/10.1016/j.isci.2021.102274>
- [14] Gan WC, Majid WHA. Enhancing pyroelectric and ferroelectric properties of PVDF composite thin films by dispersing a non-ferroelectric inclusion La₂O₃ for application in sensors. *Org Electron* 2015; 26: 121-8.
<https://doi.org/10.1016/j.orgel.2015.07.027>
- [15] Jayalakshmy M, Philip J. Pyroelectricity in strontium barium niobate/polyurethane nanocomposites for thermal/infrared detection. *Compos Sci Technol* 2015; 109: 6-11.
<https://doi.org/10.1016/j.compscitech.2015.01.007>
- [16] Ojha DP, Joshi B, Samuel E, et al. Supersonically Sprayed Flexible ZnO/PVDF Composite Films with Enhanced Piezoelectricity for Energy Harvesting and Storage. *Int J Energy Res* 2023; 2023.
<https://doi.org/10.1155/2023/3074782>
- [17] Zhang W, Wu G, Zeng H, et al. The Preparation, Structural Design, and Application of Electroactive Poly (vinylidene fluoride)-Based Materials for Wearable Sensors and Human Energy Harvesters. *Polymers* 2023; 15(13): 2766.
<https://doi.org/10.3390/polym15132766>
- [18] Yuan J, Yang X, Zheng D, et al. Perovskite quantum dot-based tandem triboelectric-solar cell for boosting the efficiency and rain energy harvesting. *Nano Energy* 2023; 110: 108341.
<https://doi.org/10.1016/j.nanoen.2023.108341>
- [19] Nie J, Zhu L, Zhai W, Berbille A, Li L, Wang ZL. Flexible piezoelectric nanogenerators based on P (VDF-TrFE)/CsPbBr₃ quantum dot composite films. *ACS Appl Electron Mater* 2021; 3(5): 2136-44.
<https://doi.org/10.1021/acsaelm.1c00137>
- [20] Devadas B, Imae T. Effect of carbon dots on conducting polymers for energy storage applications. *ACS Sustain Chem Eng* 2018; 6(1): 127-34.
<http://dx.doi.org/10.1021/acssuschemeng.7b01858>
- [21] Ahmad N, Majid WA, Zaini MS, Rosli AK, Adnan RH, Halim NA. Energy harvesting performance of a novel polymer-nanocrystal composite of P (VDF-TrFE)/ZnO QD films. *Mater Sci Eng B* 2023; 289: 116256.
<https://doi.org/10.1016/j.mseb.2022.116256>
- [22] Xu Y. *Ferroelectric materials and their applications*. Elsevier; 2013.
- [23] Batra AK, Aggarwal MD. *Pyroelectric materials: infrared detectors, particle accelerators and energy harvesters* 2013.
- [24] Mai M, Ke S, Lin P, Zeng X. Ferroelectric polymer thin films for organic electronics. *J Nanomater* 2015; 16(1): 181.
<https://doi.org/10.1155/2015/812538>
- [25] Kawai H. The piezoelectricity of poly (vinylidene fluoride). *Jpn J Appl Phys*; 8(7): 975.
- [26] Bergman Jr JG, McFee JH, Crane GR. Pyroelectricity and optical second harmonic generation in polyvinylidene fluoride films. *Appl Phys Lett* 1971; 18(5): 203-5.
<https://doi.org/10.1063/1.1653624>
- [27] Doll WW, Lando JB. Polymorphism of poly (vinylidene fluoride). III. The crystal structure of phase II. *J Macromol Sci B* 1970; 4(2): 309-29.
<https://doi.org/10.1063/1.1653624>
- [28] Furukawa T. Structure and functional properties of ferroelectric polymers. *Adv. Colloid Interface Sci* 1997; 71: 183-208.
[https://doi.org/10.1016/S0001-8686\(97\)90017-8](https://doi.org/10.1016/S0001-8686(97)90017-8)
- [29] Zhu G, Zeng Z, Zhang L, Yan X. Piezoelectricity in β -phase PVDF crystals: A molecular simulation study. *Comput Mater Sci* 2008; 44(2): 224-9.
<https://doi.org/10.1016/j.commatsci.2008.03.016>
- [30] Furukawa T. Ferroelectric properties of vinylidene fluoride copolymers. *Ph Transit: A Multinational Journal* 1989; 18(3-4): 143-211.
<https://doi.org/10.1080/01411598908206863>
- [31] Weber N, Lee YS, Shanmugasundaram S, Jaffe M, Arinze TL. Characterization and *in vitro* cytocompatibility of piezoelectric electrospun scaffolds. *Acta Biomater* 2010; 6(9): 3550-6.
<https://doi.org/10.1016/j.actbio.2010.03.035>
- [32] Jia N, He Q, Sun J, Xia G, Song R. Crystallization behavior and electroactive properties of PVDF, P (VDF-TrFE) and their blend films. *Polym Test* 2017; 57: 302-6.
<https://doi.org/10.1016/j.polymertesting.2016.12.003>
- [33] Chauhan SS, Beigh NT, Mukherjee D, Mallick D. Development and Optimization of Highly Piezoelectric BTO/PVDF-TrFE Nanocomposite Film for Energy Harvesting Application. In *2022 IEEE International Conference on Emerging Electronics (ICEE) 2022*; p. 1-5.
<https://doi.org/10.1109/ICEE56203.2022.10117949>
- [34] Kullukçu B, Bathaei M, Awais M, Mirzajani H, Beker L. Piezoelectric PVDF-TrFE/PET Energy Harvesters for Structural Health Monitoring (SHM) Applications. *Integr Ferroelectr* 2023; 237(1): 216-31.
<https://doi.org/10.1080/10584587.2023.2239101>
- [35] Kim D, Hong S, Li D, et al. A spring-type piezoelectric energy harvester. *RSC Adv* 2013; 3(10): 3194-8.
<https://doi.org/10.1039/C2RA22554A>
- [36] Apelt S, Höhne S, Mehner E, et al. Poly (vinylidene fluoride-co-trifluoroethylene) Thin Films after Dip-and Spin-Coating. *Macromol Mater Eng* 2022; 307(10): 2200296.
<https://doi.org/10.1002/mame.202200296>
- [37] Rahul MT, Chacko SK, Vinodan K, et al. Multiferroic and energy harvesting characteristics of P(VDF-TrFE)-CuFe₂O₄ flexible films. *Polymer* 2022; 14; 252: 124910.
<https://doi.org/10.1016/j.polymer.2022.124910>
- [38] Shepelin NA, Lussini VC, Fox PJ, et al. 3D printing of poly (vinylidene fluoride-trifluoroethylene): a poling-free technique to manufacture flexible and transparent piezoelectric generators. *MRS Commun* 2019; 9(1): 159-64.
<https://doi.org/10.1557/mrc.2019.19>
- [39] Koroglu L, Ayas E, Ay N. 3D Printing of Polyvinylidene Fluoride Based Piezoelectric Nanocomposites: An Overview. *Macromol Mater Eng* 2021; 306(10): 2100277.
<https://doi.org/10.1002/mame.202100277>
- [40] Rodrigues-Marinho T, Perinka N, Costa P, Lanceros-Mendez S. Printable lightweight polymer-based energy harvesting systems: materials, processes and applications. *Mater Today Sustain* 2022; 100292.
<https://doi.org/10.1016/j.mtsust.2022.100292>
- [41] Mahdi RI, Gan WC, Abd. Majid WH. Hot plate annealing at a low temperature of a thin ferroelectric P (VDF-TrFE) film with an improved crystalline structure for sensors and actuators. *Sensors* 2014; 14(10): 19115-27.
<https://doi.org/10.3390/s141019115>
- [42] Alim KA, Fonoberov VA, Shamsa M, Balandin AA. Micro-Raman investigation of optical phonons in ZnO nanocrystals. *J of Appl Phy* 2005; 97(12).
<https://doi.org/10.1063/1.1944222>
- [43] Fu YS, Du XW, Kulinich SA et al. Stable aqueous dispersion of ZnO quantum dots with strong blue emission via simple solution route. *J Am Chem Soc* 2007; 129(51): 16029-33.
<https://doi.org/10.1021/ja075604i>
- [44] Singh AK, Pal P, Gupta V, Yadav TP, Gupta V, Singh SP. Green synthesis, characterization and antimicrobial activity of zinc oxide quantum dots using *Eclipta alba*. *Mater Chem Phys* 2018; 203, 40-48.
<https://doi.org/10.1016/j.matchemphys.2017.09.049>

- [45] Kamruzzaman M. The effect of ZnO/ZnSe core/shell nanorod arrays photoelectrodes on PbS quantum dot sensitized solar cell performance. *Nanoscale Adv* 2020; 2(1): 286-95. <https://doi.org/10.1039/C9NA00523D>
- [46] Park DY, Lim JH, Ha MY, Moon DG. High efficiency quantum dot light-emitting diode by solution printing of zinc oxide nanoparticles. *J Nanosci Nanotechnol* 2020; 20(7): 4454-7. <https://doi.org/10.1166/jnn.2020.17591>
- [47] Schoenhalz AL, Arantes JT, Fazzio A, Dalpian GM. Surface and quantum confinement effects in ZnO nanocrystals. *J Phys Chem C* 2010; 114(43): 18293-7. <https://doi.org/10.1021/jp103768v>
- [48] Özgür Ü, Alivov YI, Liu C, Teke A, Reshchikov MA, Doğan S, Avrutin VC, Cho SJ, Morkoç AH. A comprehensive review of ZnO materials and devices. *J Appl Phys* 2005; 98(4). <https://doi.org/10.1063/1.1992666>
- [49] Morkoç H, Özgür Ü. Zinc oxide: fundamentals, materials and device technology. John Wiley & Sons; 2008.
- [50] Rahman F. Zinc oxide light-emitting diodes: a review. *Opt Eng* 2019; 58(1): 010901. <https://doi.org/10.1117/1.OE.58.1.010901>
- [51] Mohamed WA, Abd El-Gawad HH, Mekkey SD, Galal HR, Labib AA. Zinc oxide quantum dots: Confinement size, photophysical and tuning optical properties effect on photodecontamination of industrial organic pollutants. *Opt Mater* 2021; 118: 111242. <https://doi.org/10.1016/j.optmat.2021.111242>
- [52] Asok A, Gandhi MN, Kulkarni AR. Enhanced visible photoluminescence in ZnO quantum dots by promotion of oxygen vacancy formation. *Nanoscale* 2012; 4(16): 4943-6. <https://doi.org/10.1039/C2NR31044A>
- [53] Chen Z, Li XX, Du G, Chen N, Suen AY. A sol-gel method for preparing ZnO quantum dots with strong blue emission. *J Lumin* 2011; 131(10): 2072-7. <https://doi.org/10.1016/j.jlumin.2011.05.009>
- [54] Huang Z, Hao J, Blackburn JL, Beard MC. Pyroelectricity of Lead Sulfide (PbS) Quantum Dot Films Induced by Janus-Ligand Shells. *ACS nano* 2021; 15(9): 14965-71. <https://doi.org/10.1021/acsnano.1c05185>
- [55] Kołodziejczak-Radzimska A, Markiewicz E, Jesionowski T. Structural characterisation of ZnO particles obtained by the emulsion precipitation method. *J Nanomater* 2012; 15. <https://doi.org/10.1155/2012/656353>
- [56] Wang Z, Yu R, Pan C, *et al.* Light-induced pyroelectric effect as an effective approach for ultrafast ultraviolet nanosensing. *Nature commun* 2015; 6(1): 8401. <https://doi.org/10.1038/ncomms9401>
- [57] Fathi S, Sheikhi MH, Zerafat MM. Pyro-Phototronic Effect Coupled in Self-powered, Fast and Broadband Photodetector Based on CIS/CTS Heterojunction. *Surf Interfaces* 2023; 103283. <https://doi.org/10.1016/j.surfin.2023.103283>
- [58] Ahmed AA, Qahtan TF, Hashim MR, Nomaan AT, Al-Hardan NH, Rashid M. Eco-friendly ultrafast self-powered p-Si/n-ZnO photodetector enhanced by photovoltaic-pyroelectric coupling effect. *Ceram Int* 2022; 48(11): 16142-55. <https://doi.org/10.1016/j.ceramint.2022.02.162>
- [59] Gokana MR, Wu CM, Motora KG, Qi JY, Yen WT. Effects of patterned electrode on near infrared light-triggered cesium tungsten bronze/poly (vinylidene) fluoride nanocomposite-based pyroelectric nanogenerator for energy harvesting. *J Power Sources* 2022; 536: 231524. <https://doi.org/10.1016/j.jpowsour.2022.231524>
- [60] Jin L, Zhang Y, Cao M, *et al.* Light-induced pyroelectric property of self-powered photodetectors based on all-inorganic perovskite quantum dots. *Nanotechnology* 2021; 32(23): 235203. <https://doi.org/10.1088/1361-6528/abe672>
- [61] Bhadwal N, Ben Mrad R, Behdinin K. Review of Zinc Oxide Piezoelectric Nanogenerators: Piezoelectric Properties, Composite Structures and Power Output. *Sensors* 2023; 23(8): 3859. <https://doi.org/10.3390/s23083859>
- [62] He Q, Li X, Zhang J, Zhang H, Briscoe J. P-N junction-based ZnO wearable textile nanogenerator for biomechanical energy harvesting. *Nano Energy* 2021; 85: 105938. <https://doi.org/10.1016/j.nanoen.2021.105938>
- [63] Abubakar S, Tan ST, Liew JY, Talib ZA, Sivasubramanian R, Vaithilingam CA, Indira SS, Oh WC, Siburian R, Sagadevan S, Paiman S. Controlled Growth of Semiconducting ZnO Nanorods for Piezoelectric Energy Harvesting-Based Nanogenerators. *Nanomaterials* 2023; 13(6): 1025. <https://doi.org/10.3390/nano13061025>
- [64] Obreja P, Cristea D, Dinescu A, Romanişan C. Influence of surface substrates on the properties of ZnO nanowires synthesized by hydrothermal method. *Appl Surf Sci* 2019; 463: 1117-23. <https://doi.org/10.1016/j.apsusc.2018.08.191>
- [65] Jalali N, Briscoe J, Woolliams P, *et al.* Passivation of zinc oxide nanowires for improved piezoelectric energy harvesting devices. *J Phys: Conf Ser* 2013; 476(1): p. 012131. IOP Publishing. <https://doi.org/10.1088/1742-6596/476/1/012131>
- [66] Consonni V, Lord AM. Polarity in ZnO nanowires: A critical issue for piezotronic and piezoelectric devices. *Nano Energy* 2021; 83: 105789. <https://doi.org/10.1016/j.nanoen.2021.105789>
- [67] Li T, Li YT, Qin WW, Zhang PP, Chen XQ, Hu XF, Zhang W. Piezoelectric size effects in a zinc oxide micropillar. *Nanoscale Res Lett* 2015; 10: 1-7.
- [68] Sánchez-Godoy HE, Salim KM, Rodríguez-Rojas R, Zarazúa I, Masi S. In Situ Ethanolamine ZnO Nanoparticle Passivation for Perovskite Interface Stability and Highly Efficient Solar Cells. *Nanomaterials* 2022; 12(5): 823. <https://doi.org/10.3390/nano12050823>
- [69] Adnan RH, Woon KL, Chanlek N, Nakajima H, Majid WH. Ligand-Stabilized ZnO Quantum Dots: Molecular Dynamics and Experimental Study. *Aust J Chem* 2017; 70(10): 1110-7. <https://doi.org/10.1071/CH17078>
- [70] Dias CJ, Das-Gupta DK. Inorganic ceramic/polymer ferroelectric composite electrets. *IEEE Trans Dielectr Electr Insul* 1996; 3(5): 706-34. Available from: (<https://ieeexplore.ieee.org/stamp/stamp.jsp?arnumber=544188>)
- [71] Guggilla P, Batra AK. Novel electroceramic: polymer composites-preparation, properties and applications. *IntechOpen*; 2011. Available from: (https://www.researchgate.net/profile/AshokBatra/publication/221914421_Novel_Electroceramic_Polymer_Composites_-_Preparation_Properties_and_Applications/links/00b4952a1f6c961f90000000/Novel-Electroceramic-Polymer-Composites-Preparation-Properties-and-Applications.pdf)
- [72] Slabov V, Kopyl S, Soares dos Santos MP, Kholkin AL. Natural and eco-friendly materials for triboelectric energy harvesting. *Nanomicro Lett* 2020; 12: 1-8. <https://doi.org/10.1007/s40820-020-0373-y>
- [73] Cai C, Luo B, Liu Y, Fu Q, Liu T, Wang S, Nie S. Advanced triboelectric materials for liquid energy harvesting and emerging application. *Materials Today* 2022; 52: 299-326. <https://doi.org/10.1016/j.mattod.2021.10.034>
- [74] Kim J, Lee JH, Ryu H, *et al.* High-performance piezoelectric, pyroelectric, and triboelectric nanogenerators based on P(VDF-TrFE) with controlled crystallinity and dipole alignment. *Adv Funct Mater* 2017; 27(22): 1700702. <https://doi.org/10.1002/adfm.201700702>
- [75] Gunasekhar R, Sathiyathanan P, Reza MS, Prasad G, Prabu AA, Kim H. Polyvinylidene Fluoride/Aromatic Hyperbranched Polyester of Third-Generation-Based Electrospun Nanofiber as a Self-Powered Triboelectric Nanogenerator for Wearable Energy Harvesting and Health Monitoring Applications. *Polymers* 2023; 15(10): 2375. <https://doi.org/10.3390/polym15102375>
- [76] Javed R, Zia M, Naz S, Aisida SO, Ain NU, Ao Q. Role of capping agents in the application of nanoparticles in biomedicine and environmental remediation: recent trends and future prospects. *J Nanobiotechnology* 2020; 18: 1-5. <https://doi.org/10.1186/s12951-020-00704-4>

- [77] Korlacki R, Saraf RF, Ducharme S. Electrical control of photoluminescence wavelength from semiconductor quantum dots in a ferroelectric polymer matrix. *Appl Phys Lett* 2011; 99(15). <http://dx.doi.org/10.1063/1.3651322>
- [78] Zhang X, Xu J, Shi S, *et al.* Ferroelectric-like hysteresis effect observed in carbon quantum dots sandwiched between PMMA and PEDOT: PSS hybrid film. *RSC Adv* 2016; 6(63): 58733-9.
- [79] Ahmed RM, Morsi RM. Polymer nanocomposite dielectric and electrical properties with quantum dots nanofiller. *Mod Phys Lett B* 2017; 31(30): 1750278. <https://doi.org/10.1142/S0217984917502785>
- [80] Li L, Cheng J, Cheng Y *et al.* Polymer dielectrics exhibiting an anomalously improved dielectric constant simultaneously achieved high energy density and efficiency enabled by CdSe/Cd 1- x Zn x S quantum dots. *J Mater Chem A* 2020; 8(27): 13659-70. <https://doi.org/10.1039/d0ta02760j>
- [81] Kao KC. Dielectric phenomena in solids. Elsevier; 2004. Available from: (https://cds.cern.ch/record/824239/files/0123965616_TOC.pdf)
- [82] Lu J, Wong CP. Nanoparticle-based high-k dielectric composites: opportunities and challenges. *Nanopackaging: nanotechnologies and electronics packaging* 2008; 121-37.
- [83] Usman M. Studies of Ferroelectric and Multiferroic Behavior in [Ba (Zr, Ti) O₃] 1-y: [CoFe₂O₄] y System (Doctoral dissertation, Quaid-i-Azam University, Islamabad).
- [84] Kremer F, Schönhals A, editors. Broadband dielectric spectroscopy. Springer Science & Business Media; 2002.
- [85] Furukawa T, Johnson GE. Dielectric relaxations in a copolymer of vinylidene fluoride and trifluoroethylene. *J Appl Phys* 1981; 52(2): 940-3.
- [86] Gan WC. Ferroelectric and pyroelectric properties of form IV Poly (Vinylidene Fluoride) and its composites/Gan Wee Chen (Doctoral dissertation, University of Malaya).
- [87] Arshad AN, Wahid MH, Rusop M, Majid WH, Subban RH, Rozana MD. Dielectric and structural properties of poly (vinylidene fluoride)(PVDF) and poly (vinylidene fluoride-trifluoroethylene)(PVDF-TrFE) filled with magnesium oxide nanofillers. *J Nanomater* 2019; 2019. <https://doi.org/10.1155/2019/5961563>
- [88] Li J, Zhao C, Xia K, Liu X, Li D, Han J. Enhanced piezoelectric output of the PVDF-TrFE/ZnO flexible piezoelectric nanogenerator by surface modification. *Appl Surf Sci* 2019; 463: 626-34. <https://doi.org/10.1016/j.apsusc.2018.08.266>
- [89] Tan KS, Gan WC, Velayutham TS, Abd Majid WH. Pyroelectricity enhancement of PVDF nanocomposite thin films doped with ZnO nanoparticles. *Smart mater struct* 2014; 23(12): 125006. <https://doi.org/10.1088/0964-1726/23/12/125006>
- [90] Vo HT, Shi FG. Towards model-based engineering of optoelectronic packaging materials: dielectric constant modeling. *Microelectronics journal* 2002 May 6; 33(5-6): 409-15.
- [91] Sahoo R, Singh NK, Bajpai V. A novel approach for modeling MRR in EDM process using utilized discharge energy. *Mech Syst Signal Process* 2023; 185: 109811. <https://doi.org/10.1016/j.ymssp.2022.109811>
- [92] Mahdi RI, Gan WC, Abd Majid WH, Mukri NI, Furukawa T. Ferroelectric polarization and pyroelectric activity of functionalized P (VDF-TrFE) thin film lead free nanocomposites. *Polymer* 2018; 141: 184-93. <https://doi.org/10.1016/j.polymer.2018.03.004>
- [93] Ploss B, Ploss B, Shin FG, Chan HL, Choy CL. Pyroelectric activity of ferroelectric PT/PVDF-TRFE. *IEEE transactions on dielectrics and electrical insulation* 2000; 7(4): 517-22.
- [94] Ng KL, Chan HL, Choy CL. Piezoelectric and pyroelectric properties of PZT/P (VDF-TrFE) composites with constituent phases poled in parallel or antiparallel directions. *IEEE transactions on ultrasonics, ferroelectrics, and frequency control* 2000; 47(6): 1308-15. <https://doi.org/10.1109/58.883519>
- [95] Suresh MB, Yeh TH, Yu CC, Chou CC. Dielectric and ferroelectric properties of polyvinylidene fluoride (PVDF)-Pb_{0.52}Zr_{0.48}TiO₃ (PZT) nano composite films. *Ferroelectrics* 2009; 381(1): 80-6.
- [96] Ahmad N, Majid WA, Zaini MS, Rosli AK, Adnan RH, Halim NA. Energy harvesting performance of a novel polymer-nanocrystal composite of P(VDF-TrFE)/ZnO QD films. *Mater Sci Eng B* 2023; 289: 116256. <https://doi.org/10.1016/j.mseb.2022.116256>
- [97] Dash S, Choudhary RN, Goswami MN. Enhanced dielectric and ferroelectric properties of PVDF-BiFeO₃ composites in 0-3 connectivity. *J Alloys Compd* 2017; 715: 29-36. <https://doi.org/10.1016/j.jallcom.2017.04.310>
- [98] Lang, S. B. (1974). Sourcebook of Pyroelectricity, Gordon and Breach. New York.
- [99] Furukawa T, Wen JX, Suzuki K, Takashina Y, Date M. Piezoelectricity and pyroelectricity in vinylidene fluoride/trifluoroethylene copolymers. *J Appl Phys* 1984; 56(3): 829-34.
- [100] Bowen CR, Taylor J, Le Boulbar E, Zabek D, Topolov VY. A modified figure of merit for pyroelectric energy harvesting. *Mater Lett* 2015; 138: 243-6. <https://doi.org/10.1016/j.matlet.2014.10.004>
- [101] Lang SB. Pyroelectricity: from ancient curiosity to modern imaging tool. *Phys Today* 2005; 58(8): 31-6.
- [102] Kishore RA, Priya S. A review on low-grade thermal energy harvesting: Materials, methods and devices. *Mater* 2018; 11(8): 1433. <https://doi.org/10.3390/ma11081433>
- [103] Tichy J, Erhart J, Kittinger E, Privratska J. Fundamentals of piezoelectric sensorics: mechanical, dielectric, and thermodynamical properties of piezoelectric materials. Springer Science & Business Media; 2010.
- [104] Majid WA, Richardson TH, Lacey D, Topacli A. Qualitative evaluation of pyroelectric mechanisms in Langmuir-Blodgett films containing a cyclic polysiloxane substituted with aliphatic side chains using Fourier transform infrared (FTIR) spectroscopy. *Thin Solid Films* 2000; 376(1-2): 225-31.
- [105] WC G, Majid WH. The effect of gases on pyroelectric properties of PVDF/TiO₂ treated by plasma etcher. *Trans Mater Res Soc Jpn* 2009; 34(1): 67-71.
- [106] Mahdi RI, Majid WA. Piezoelectric and pyroelectric properties of BNT-base ternary lead-free ceramic-polymer nanocomposites under different poling conditions. *RSC Adv* 2016; 6(84): 81296-309. <https://doi.org/10.1039/C6RA12033D>
- [107] Navid A, Lynch CS, Pilon L. Purified and porous poly (vinylidene fluoride-trifluoroethylene) thin films for pyroelectric infrared sensing and energy harvesting. *Smart Mater Struct* 2010; 19(5): 055006. <https://doi.org/10.1088/0964-1726/19/5/055006>
- [108] Gan WC, Majid WH. Enhancing pyroelectric and ferroelectric properties of PVDF composite thin films by dispersing a non-ferroelectric inclusion La₂O₃ for application in sensors. *Org Electron* 2015; 26: 121-8. <https://doi.org/10.1016/j.orgel.2015.07.027>
- [109] Yang Y, Guo W, Pradel KC, Zhu G, Zhou Y, Zhang Y, Hu Y, Lin L, Wang ZL. Pyroelectric nanogenerators for harvesting thermo-electric energy. *Nano Lett* 2012; 12(6): 2833-8. <https://doi.org/10.1021/nl3003039>
- [110] Anand A, Bhatnagar MC. Role of vertically aligned and randomly placed zinc oxide (ZnO) nanorods in PVDF matrix: Used for energy harvesting. *Mater Today Energy* 2019; 13: 293-301. <https://doi.org/10.1016/j.mtener.2019.06.005>
- [111] Ryu H, Kim SW. Emerging pyroelectric nanogenerators to convert thermal energy into electrical energy. *Small* 2021; 17(9): 1903469. <https://doi.org/10.1002/sml.201903469>
- [112] Xue H, Yang Q, Wang D, *et al.* A wearable pyroelectric nanogenerator and self-powered breathing sensor. *Nano Energy* 2017; 38: 147-54. <https://doi.org/10.1016/j.nanoen.2017.05.056>

- [113] Iwamoto M, Taguchi D. Research trend in thermally stimulated current method for development of materials and devices in Japan. *Jpn J Appl Phys* 2018; 57(3S2): 03EA04. <https://doi.org/10.7567/JJAP.57.03EA04>
- [114] Van Turnhout J. Thermally stimulated discharge of polymer electrets. *Polymer Journal*. 1971; 2(2): 173-91.
- [115] Belana J, Pujal M, Colomer P, Montserrat S. Cold crystallization effect on α and ρ amorphous poly (ethylene terephthalate) relaxations by thermally stimulated discharge currents. *Polymer* 1988; 29(10): 1738-44.
- [116] Mizutani T, Yamada T, Ieda M. Thermally stimulated currents in polyvinylidene fluoride. I. Unstretched alpha-form PVDF. *J Phys D: Appl Phys* 1981; 14(6): 1139.
- [117] Van Turnhout J. Thermally stimulated discharge of electrets. *Electrets* 2005: 81-215.
- [118] Capsal JF, Dantras E, Lacabanne C. Molecular mobility interpretation of the dielectric relaxor behavior in fluorinated copolymers and terpolymers. *J Non Cryst Solids* 2013; 363: 20-5. <https://doi.org/10.1016/j.jnoncrysol.2012.12.008>
- [119] Ahmad N, Majid WA, Halim NA. Thermally Stimulated Current Study and Relaxation Behaviour of Annealed Copolymer P (VDF-TrFE) Films for Potential Pyroelectric Energy Harvesting. *J Electron Mater* 2020; 49(9): 5585-99.
- [120] Diogo HP, Ramos JJ. Slow molecular mobility in the crystalline and amorphous solid states of glucose as studied by thermally stimulated depolarization currents (TSDC). *Carbohydr Res* 2008; 343(16): 2797-803. <https://doi.org/10.1016/j.carres.2008.07.002>
- [121] Sature KR, Patil BJ, Dahiwalé SS, Bhoraskar VN, Dhole SD. Development of computer code for deconvolution of thermoluminescence glow curve and DFT simulation. *J Lumin* 2017; 192: 486-95. <https://doi.org/10.1016/j.jlumin.2017.06.016>
- [122] Yamada T, Mizutani T, Ieda M. Thermally stimulated currents in polyvinylidene fluoride. II. Effects of stretching. *J Phys D: Appl Phys* 1982; 15(2): 289.
- [123] Teyssedre G, Lacabanne C. Study of the thermal and dielectric behavior of P (VDF-TrFE) copolymers in relation with their electroactive properties. *Ferroelectrics* 1995; 171(1): 125-44.
- [124] Hughes ST, Piercy AR. Study of pyroelectric and relaxation phenomena in poly (vinylidene fluoride) using thermal current analysis. *J Phys D: Appl Phys* 1987; 20(9): 1175.
- [125] Mizutani T, Yamada T, Ieda M. Thermally stimulated currents in polyvinylidene fluoride. I. Unstretched alpha-form PVDF. *Journal of Physics D: Applied Physics*. 1981; 14(6): 1139.
- [126] Teyssedre G, Bernes A, Lacabanne C. DSC and TSC study of a VDF/TrFE copolymer. *Thermochimica acta*. 1993 Oct 26; 226: 65-75.
- [127] Bruzzi M, Gabelloni F, Calisi N, Caporali S, Vinattieri A. Defective states in micro-crystalline CsPbBr₃ and their role on photoconductivity. *Nanomaterials* 2019; 9(2): 177. <https://doi.org/10.3390/nano9020177>
- [128] Kielar M, Daanouné M, François-Martin O, *et al.* Insights into the failure mechanisms of organic photodetectors. *Adv Electron Mater* 2018; 4(2): 1700526. <https://doi.org/10.1002/aelm.201700526>

Received on 20-08-2023

Accepted on 10-09-2023

Published on 04-10-2023

<https://doi.org/10.6000/1929-5995.2023.12.12>© 2023 Majid *et al.*; Licensee Lifescience Global.

This is an open-access article licensed under the terms of the Creative Commons Attribution License (<http://creativecommons.org/licenses/by/4.0/>), which permits unrestricted use, distribution, and reproduction in any medium, provided the work is properly cited.